Cell Reports
Methods

Article

# High-efficiency pharmacogenetic ablation of oligodendrocyte progenitor cells in the adult mouse CNS

## Graphical abstract

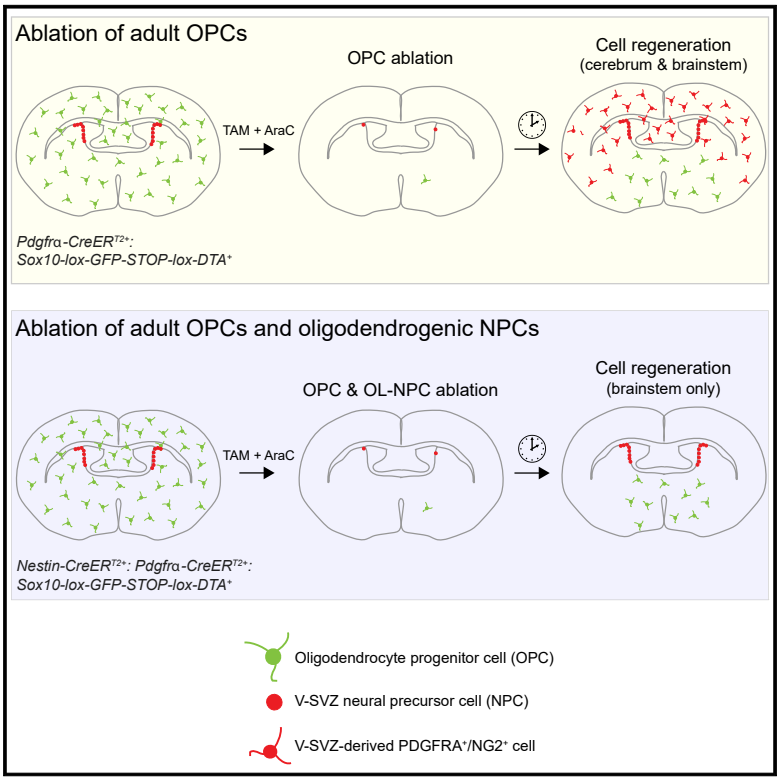


## Highlights

- A pharmacogenetic approach to ablate OPCs in the adult mouse CNS
- Method ablates >98% of OPCs in the brain
- PDGFRA$^+$/NG2$^+$ cells start to regenerate within 12 days post ablation
- Cells repopulating the cerebrum derive mainly from neural progenitors in the V-SVZ

## Authors

Yao Lulu Xing, Jasmine Poh, Bernard H.A. Chuang, ..., Trevor J. Kilpatrick, Yasuyuki Osanai, Tobias D. Merson

## Correspondence

toby.merson@nih.gov

## In brief

Xing et al. report the development of a pharmacogenetic method to ablate almost all oligodendrocyte progenitor cells (OPCs) from the adult mouse brain. PDGFRA$^+$NG2$^+$ cells that repopulate the cerebrum derive principally from the ventricular-subventricular zone. The model will serve as a valuable resource to study the function of OPCs.

Xing et al., 2023, Cell Reports Methods 3, 100414
February 27, 2023
https://doi.org/10.1016/j.crmeth.2023.100414

CellPress

Cell Reports Methods

CellPress
OPEN ACCESS

Article

# High-efficiency pharmacogenetic ablation of oligodendrocyte progenitor cells in the adult mouse CNS

Yao Lulu Xing,[1,5] Jasmine Poh,[1] Bernard H.A. Chuang,[1] Kaveh Moradi,[1,2,6] Stanislaw Mitew,[1] William D. Richardson,[3] Trevor J. Kilpatrick,[2,4] Yasuyuki Osanai,[1,7] and Tobias D. Merson[1,8,9,*]

[1]Australian Regenerative Medicine Institute, Monash University, Clayton, VIC 3800, Australia
[2]Florey Institute of Neuroscience and Mental Health, Parkville, VIC 3052, Australia
[3]Wolfson Institute for Biomedical Research, University College London, London WC1E 6BT, UK
[4]Florey Department of Neuroscience and Mental Health, The University of Melbourne, Parkville, VIC 3052, Australia
[5]Present address: Department of Neurosurgery, Stanford University School of Medicine, Stanford, CA 94305, USA
[6]Present address: Department of Anatomy and Neurobiology, Virginia Commonwealth University, Richmond, VA 23298, USA
[7]Present address: Division of Histology and Cell Biology, Department of Anatomy, Jichi Medical University, Tochigi 329-0498, Japan
[8]Present address: National Institute of Mental Health, National Institutes of Health, Bethesda, MD 20892, USA
[9]Lead contact
*Correspondence: toby.merson@nih.gov
https://doi.org/10.1016/j.crmeth.2023.100414

**MOTIVATION** To investigate the function of oligodendrocyte progenitor cells (OPCs), several groups have developed strategies to deplete OPCs within the adult CNS. However, these methods have significant limitations in achieving complete or long-term OPC ablation. We developed a pharmacogenetic method that achieves near-complete ablation of OPCs via the inducible and conditional expression of diphtheria toxin A (DTA) in adult OPCs followed by delivery of an anti-mitotic agent into the CNS to ablate dividing OPCs that escape genetic targeting.

## SUMMARY

Approaches to investigate adult oligodendrocyte progenitor cells (OPCs) by targeted cell ablation in the rodent CNS have limitations in the extent and duration of OPC depletion. We have developed a pharmacogenetic approach for conditional OPC ablation, eliminating >98% of OPCs throughout the brain. By combining recombinase-based transgenic and viral strategies for targeting OPCs and ventricular-subventricular zone (V-SVZ)-derived neural precursor cells (NPCs), we found that new PDGFRA-expressing cells born in the V-SVZ repopulated the OPC-deficient brain starting 12 days after OPC ablation. Our data reveal that OPC depletion induces V-SVZ-derived NPCs to generate vast numbers of PDGFRA$^{+}$NG2$^{+}$ cells with the capacity to proliferate and migrate extensively throughout the dorsal anterior forebrain. Further application of this approach to ablate OPCs will advance knowledge of the function of both OPCs and oligodendrogenic NPCs in health and disease.

## INTRODUCTION

Oligodendrocyte progenitor cells (OPCs) are the principal mitotic cell type in the adult mammalian CNS. OPCs are known primarily for generating myelin-forming oligodendrocytes (OLs) during postnatal development and adulthood.[1,2] Although OPCs are distributed throughout the CNS, including in brain regions where relatively little myelination occurs, there is evidence of OPC heterogeneity among brain regions,[3,4] raising the prospect that they could possess additional functions beyond oligodendrogenesis.

To investigate OPC function, several groups have developed strategies to selectively ablate OPCs, including X-irradiation, laser-mediated ablation, genetically induced cell ablation, or the use of anti-mitotic drugs.[5–10] However these approaches have enabled only partial and transient OPC ablation because of incomplete targeting of the OPC population and rapid repopulation by non-ablated OPCs. Consequently, it has not yet been possible to explore the functional consequences of long-term OPC ablation.

Designing a genetic approach to selectively ablate OPCs requires careful consideration of the promoter(s) used for OPC


This is an open access article under the CC BY-NC-ND license (http://creativecommons.org/licenses/by-nc-nd/4.0/).

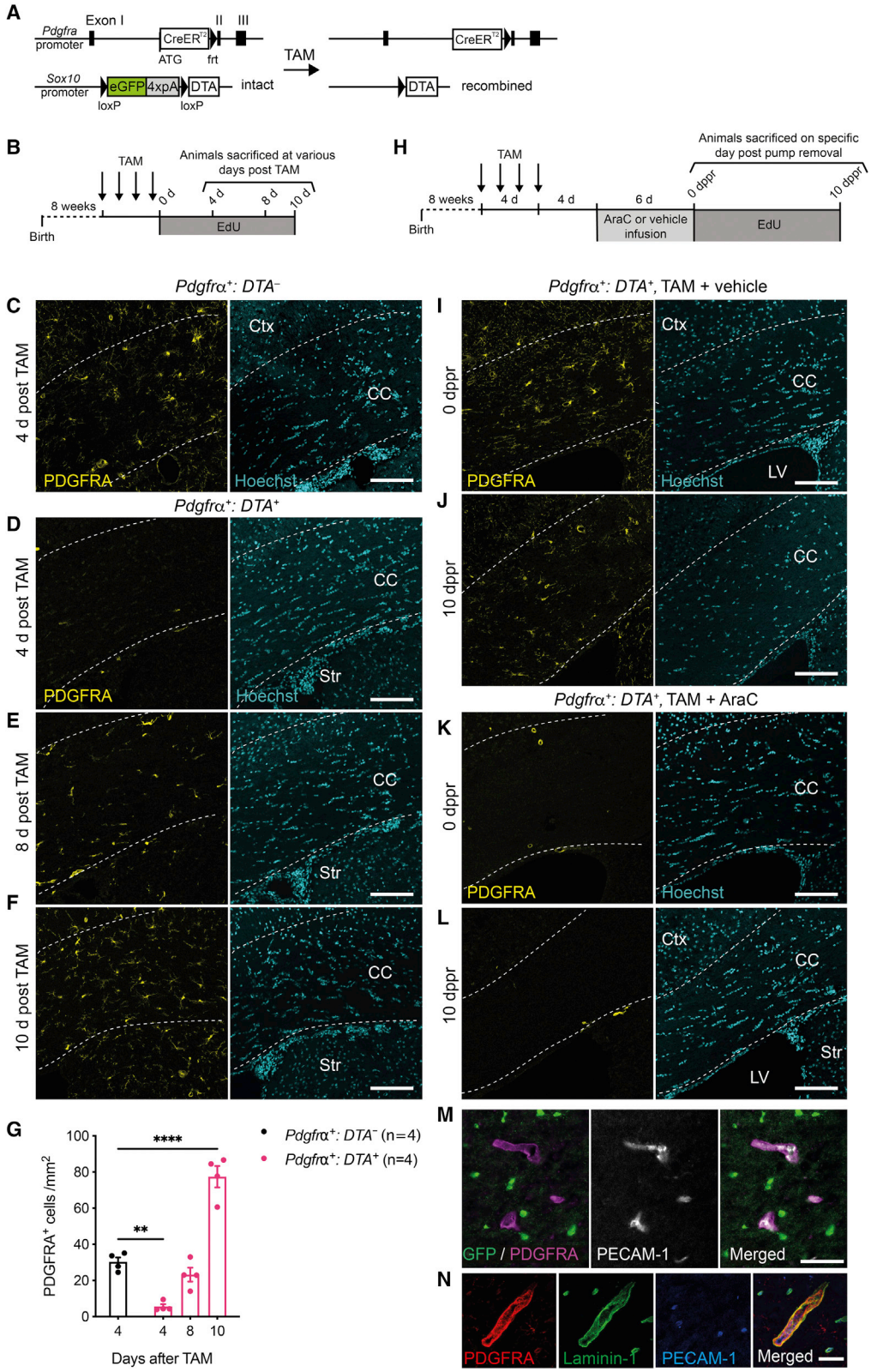


*(legend on next page)*

targeting. OPCs are defined by their expression of chondroitin sulfate proteoglycan 4 (CSPG4)/neuron-glial antigen 2 (NG2)[11] and platelet-derived growth factor receptor alpha (PDGFRA).[12] Although the *Cspg4* promoter has been used to control transgene expression,[1,8,13,14] NG2 is also expressed by pericytes[7,9,15,16] and some microglia after injury.[17] PDGFRA is also expressed by vascular and leptomeningeal cells (VLMCs)[15,16] and choroid plexus epithelial cells.[1,18,19] Therefore, using either the *Cspg4* or *Pdgfra* promoter alone cannot direct the expression of a suicide gene exclusively to OPCs. To precisely target OPCs we have generated a novel transgenic mouse model in which the expression of an inducible suicide gene is controlled by two different promoters, namely, the *Pdgfra* and *Sox10* promoters, whose overlapping transcriptional activity is restricted to OPCs in the postnatal CNS.

The method to conditionally ablate OPCs must also be highly efficient to overcome the proliferation of non-ablated OPCs that follows incomplete OPC ablation.[6–8] Moreover, the method should be amenable to precise temporal control and have minimal effect on the animal's overall health. To date, no strategy for ablating the OPC population has been described that meets all these requirements. Here we describe the development of a highly efficient pharmacogenetic approach to ablate OPCs in the adult mouse CNS that overcomes many limitations of previous approaches. The model provides a valuable tool for studies aimed at better understanding the functions of OPCs in the adult CNS.

## RESULTS

### DTA-mediated ablation of OPCs induced rapid OPC regeneration

To specifically ablate OPCs in the adult mouse CNS, we used an intersectional genetic approach to direct the inducible expression of a suicide gene in cells expressing both PDGFRA and SOX10. This was achieved by crossing two transgenic mouse lines, the *Pdgfrα-CreER$^{T2}$* line[12] and the *Sox10-lox-GFP-STOP-lox-DTA* (*Sox10-DTA*) line,[20] to enable diphtheria toxin A (DTA) expression in adult OPCs upon delivery of tamoxifen (TAM) (Figure 1A). As SOX10 is expressed exclusively by oligodendroglia in the postnatal CNS,[21,22] this ensures that DTA expression is restricted to OPCs and is excluded from VLMCs and choroid plexus epithelial cells, which express PDGFRA but not SOX10. DTA expression is not expected to target Schwann cells in the peripheral nervous system since most Schwann cells express SOX10 but not PDGFRA.[23,24] Moreover, it has been demonstrated conclusively that the *Pdgfrα-CreER$^{T2}$* line used in our study does not target Schwann cells.[25]

TAM was administered to 8-week-old *Pdgfrα-CreER$^{T2+/+}$:Sox10-DTA$^{+/-}$* mice (hereafter denoted *Pdgfrα$^{+}$:DTA$^{+}$*), and *Pdgfrα-CreER$^{T2+/+}$:Sox10-DTA$^{-/-}$* littermates lacking the *Sox10-DTA* allele (denoted *Pdgfrα$^{+}$:DTA$^{-}$*), which served as non-ablated controls (Figure 1B). Immunohistochemistry on brains of non-ablated *Pdgfrα$^{+}$:DTA$^{-}$* controls sacrificed 4 days post-TAM revealed abundant PDGFRA$^{+}$ OPCs throughout the brain, including the corpus callosum (Figure 1C). By contrast, TAM-administered *Pdgfrα$^{+}$:DTA$^{+}$* mice assessed at the same time point had very few PDGFRA$^{+}$ OPCs in the corpus callosum (Figure 1D), suggesting that Cre-mediated induction of DTA expression resulted in OPC ablation. In these OPC-deficient mice, *Sox10* promoter-driven GFP expression was restricted to SOX10$^{+}$CC1$^{+}$ cells (Figures S1A and S1B), indicating that Cre-mediated recombination of the *Sox10-DTA* allele targeted OPCs but not mature OLs.

Although *Pdgfrα$^{+}$:DTA$^{+}$* mice exhibited marked OPC depletion 4 days post-TAM, OPC density in the corpus callosum returned to control levels by day 8 post-TAM and increased further over the subsequent 2 days (Figures 1E–1G). The marked increase in OPC density observed 10 days post-TAM suggests that OPCs exhibit robust proliferation following acute ablation. Indeed, most OPCs present after 10 days were newly generated, as demonstrated by the significant proportion of PDGFRA$^{+}$ cells incorporating 5-ethynyl-2′-deoxyuridine (EdU) provided continuously in the drinking water after TAM delivery (Figures S1C and S1D). Most OPCs present 4 days post-TAM expressed GFP (Figure S1D), suggesting that surviving OPCs were principally those in which the *Sox10-DTA* allele had not recombined. Some EdU$^{+}$ OPCs did not express GFP (Figure S1D), most likely reflecting low transcriptional activity of the *Sox10* promoter that directs GFP expression. Supporting this idea, not all SOX10$^{+}$ oligodendroglia in *Pdgfrα$^{+}$:DTA$^{+}$* brains examined 4 days post-TAM expressed GFP (Figure S1A). Together, these data demonstrate that the vast majority of OPCs in *Pdgfrα$^{+}$:DTA$^{+}$* mice were depleted after TAM administration. However, residual non-recombined OPCs exhibited a robust proliferative response to OPC ablation, resulting in restoration of OPCs to similar or higher density than non-ablated controls within 8–10 days post-TAM.

**Figure 1. TAM administration followed by intracisternal infusion of AraC to *Pdgfrα$^{+}$:DTA$^{+}$* mice ablates almost all OPCs in the brain**

(A) Schematic diagram of the transgenic alleles in *Pdgfrα$^{+}$:DTA$^{+}$* mice.

(B) Experimental timeline for TAM administration.

(C) Coronal brain section of a TAM-administered *Pdgfrα$^{+}$:DTA$^{-}$* mouse immunolabeled with an antibody against PDGFRA.

(D) Lack of PDGFRA$^{+}$ OPCs in the corpus callosum of a *Pdgfrα$^{+}$:DTA$^{+}$* mouse sacrificed 4 days post-TAM.

(E and F) Regeneration of PDGFRA$^{+}$ OPCs at days 8 and 10 post-TAM.

(G) Density of callosal PDGFRA$^{+}$ OPCs post-TAM.

(H) Experimental timeline for TAM + AraC administration.

(I and J) Callosal OPC repopulation in vehicle-infused *Pdgfrα$^{+}$:DTA$^{+}$* mice.

(K and L) OPC repopulation was not observed in AraC-infused mice at either 0 or 10 dppr.

(M and N) Residual PDGFRA-expressing cells in an AraC-infused mouse at 10 dppr were identified as VLMCs on the basis of their close association with PECAM-1-labelled endothelial cells (M) and colocalization of PDGFRA and Laminin-1 (N).

CC, corpus callosum; Ctx, cerebral cortex; LV, lateral ventricle; TAM, tamoxifen. Data represent mean ± SEM. Two-way ANOVA with Dunnett's multiple-comparison tests (G); **$p < 0.01$ and ****$p < 0.0001$. Scale bars, 100 μm (C–F, I–L), 50 μm (M), and 30 μm (N).

See also Figure S1.

### Intracisternal infusion of AraC following TAM prevented rapid OPC regeneration

Given that incomplete OPC ablation triggered non-recombined OPCs that had escaped DTA-mediated apoptosis to proliferate and repopulate the CNS, we introduced a second intervention designed to kill these rapidly dividing OPCs. After TAM administration, the anti-mitotic cytosine-β-D-arabinofuranoside (AraC) was infused into the cisterna magna of *Pdgfrα*$^{+}$*:DTA*$^{+}$ mice to deplete proliferating OPCs. We elected to administer AraC directly into the cerebrospinal fluid rather than providing additional doses of TAM, given that we have noted toxicity when administering TAM for more than 4 days. Osmotic minipumps were implanted on day 4 post-TAM and removed on day 10 (Figure 1H), to provide 6 days of AraC infusion during the period of marked OPC proliferation. Vehicle-only controls received artificial cerebrospinal fluid (aCSF) without AraC. Mice were sacrificed either immediately after removal of the osmotic minipump or 10 days later (Figure 1H).

TAM-administered *Pdgfrα*$^{+}$*:DTA*$^{+}$ mice examined after 6 days of vehicle infusion, denoted as 0 days post-pump removal (dppr), had numerous PDGFRA$^{+}$ OPCs in the corpus callosum (Figure 1I), similar in density to that observed in *Pdgfrα*$^{+}$*:DTA*$^{+}$ mice administered TAM alone and assessed 10 days later (Figure 1F). By contrast, no PDGFRA$^{+}$ OPCs could be identified in the corpus callosum of TAM-administered *Pdgfrα*$^{+}$*:DTA*$^{+}$ mice sacrificed immediately after AraC infusion (Figure 1K). Indeed, we did not observe any OPCs in the cerebrum of OPC-ablated mice in sections of the rostral forebrain examined at 0 dppr, and only occasionally did we detect OPCs in the brainstem.

Following ablation, OPCs remained depleted for at least 10 days post-AraC infusion (Figure 1L). Notably, AraC delivery to wild-type mice did not result in OPC loss (Figure S1F), consistent with the low proliferation rate of OPCs under basal conditions[15,26] and known homeostatic control mechanisms that maintain OPC density in equilibrium.[6] Although PDGFRA$^{+}$ OPCs were almost completely absent in TAM + AraC-administered *Pdgfrα*$^{+}$*:DTA*$^{+}$ mice, vascular-associated PDGFRA$^{+}$GFP$^{-}$ cells surrounding PECAM-1$^{+}$ endothelial cells remained intact (Figure 1M). Vascular-associated PDGFRA$^{+}$GFP$^{-}$ cells in OPC-ablated mice did not exhibit typical ramified OPC morphology. We identified these cells as laminin-1$^{+}$ VLMCs that are closely associated with but distinct from vascular-associated NG2$^{+}$PDGFRB$^{+}$ pericytes (Figures 1N and S1G–S1J), consistent with the recent description of these cells.[16]

To further explore the extent of OPC ablation, we generated *Pdgfrα-CreER*$^{T2+/-}$*:Ai14-tdTomato*$^{+/-}$*:Sox10-DTA*$^{+/-}$ mice (hereafter denoted *Pdgfrα*$^{+}$*:tdT*$^{+}$*:DTA*$^{+}$), to enable simultaneous genetic fate-mapping and ablation of OPCs. TAM was administered to 8-week-old *Pdgfrα*$^{+}$*:tdT*$^{+}$*:DTA*$^{+}$ mice to induce expression of both tdTomato and DTA from the *Ai14 tdTomato* and *Sox10-DTA* recombined alleles, respectively (Figure 2A). Starting 4 days post-TAM, mice received a 6-day infusion of AraC before being sacrificed. *Pdgfrα*$^{+}$*:tdT*$^{+}$*:DTA*$^{-}$ littermates administered TAM and infused with vehicle alone served as non-ablated controls. At the end of vehicle infusion, 97.0% ± 0.6% of PDGFRA$^{+}$ OPCs in non-ablated controls expressed tdTomato (Figures 2B and 2E), irrespective of differences in the local density of PDGFRA$^{+}$ OPCs along the rostrocaudal axis of the brain (Figure 2F). Cellular morphology was used to discriminate between OPCs and VLMCs, the former possessing fine ramified processes whereas the latter were devoid of fine processes and exhibited a circular morphology consistent with vascular localization. We also identified numerous tdTomato$^{+}$CC1$^{+}$ OLs generated by these fate-mapped OPCs in non-ablated controls (Figure 2D). By contrast, virtually no tdTomato$^{+}$PDGFRA$^{+}$ cells exhibiting typical OPC morphology were detected in the brains of *Pdgfrα*$^{+}$*:tdT*$^{+}$*:DTA*$^{+}$ mice administered TAM + AraC (Figures 2B, 2F, and S2A lower panels) with only perivascular tdTomato$^{+}$PDGFRA$^{+}$ cells remaining (Figures S2B and S2C). The mean density of tdTomato$^{+}$ OPCs in the AraC-infused brains was 99.7% ± 0.2% lower than that observed in vehicle-infused brains (0.16 ± 0.07 versus 70.1 ± 5.8 cells/mm$^{2}$, $p < 0.0001$). We also identified significantly fewer non-recombined (tdTomato$^{-}$) OPCs in ablated mice compared with non-ablated controls (0.53 ± 0.14 versus 2.3 ± 0.2 cells/mm$^{2}$, $p < 0.0001$) (Figure 2G). When tdTomato$^{+}$ and tdTomato$^{-}$ OPC counts were combined, this equated to a 98.6% ± 0.4% reduction in total OPC density across the entire brain of OPC-ablated mice compared with non-ablated control mice at 0 dppr ($p < 0.0001$) (Figure 2H). By 10 dppr, the mean density of tdTomato$^{+}$ OPCs in ablated mice had increased marginally but remained 97.1% ± 0.6% lower than that observed in vehicle-infused mice (2.00 ± 0.93 versus 70.1 ± 5.8 cells/mm$^{2}$, $p < 0.0001$). At this time point, PDGFRA$^{+}$ cells remained depleted in the cerebrum, but began to repopulate caudoventral regions of the brain, particularly the brainstem (Figure S2D). By 20 dppr, PDGFRA$^{+}$ cells were evident in both the brainstem and cerebrum (Figures S2E and S2F). Collectively, our results demonstrate highly efficient OPC ablation throughout the brain that persists for at least 10 dppr after which PDGFRA$^{+}$ cells started to reappear, first in the brainstem then later in the cerebrum.

### Effects of OPC ablation on specific cell types in the brain

To assess whether the induction of DTA-mediated apoptosis was restricted to OPCs within the oligodendroglial lineage, we quantified the densities of CC1$^{+}$ mature OLs in coronal brain sections of OPC-ablated and non-ablated controls. We observed similar OL densities between groups (Figures 3A–3C). The transient ablation of PDGFRA$^{+}$NG2$^{+}$ cells resulted in a complete yet temporary disruption in oligodendrogenesis. This was evaluated by quantitating the density of ASPA$^{+}$EdU$^{+}$ cells in the corpus callosum of OPC-ablated and non-ablated controls that were administered EdU continuously in their drinking water following infusion, until they were perfused at either 11, 20, or 34 dppr (Figure 3D). Consistent with this finding, the corpus callosum was deficient in both early (PDGFRA$^{+}$ GPR17$^{-}$) and late (PDGFRA$^{+}$ GPR17$^{+}$) OPCs as well as committed oligodendrocyte progenitors (PDGFRA$^{-}$ GPR17$^{+}$) that are in the process of transitioning into mature OLs for at least 10 dppr before returning to control levels by 20 dppr (Figures S3A and S3B). Despite the transient reduction in oligodendrogenesis, the absolute density of callosal ASPA$^{+}$ OLs was not significantly different from non-ablated controls (Figure 3C), and no differences in myelin abundance were detected (Figures 3E and 3F). Together these findings suggest that OPC ablation resulted in a transient disruption to the production of newborn oligodendroglia but did not affect pre-existing mature OLs.

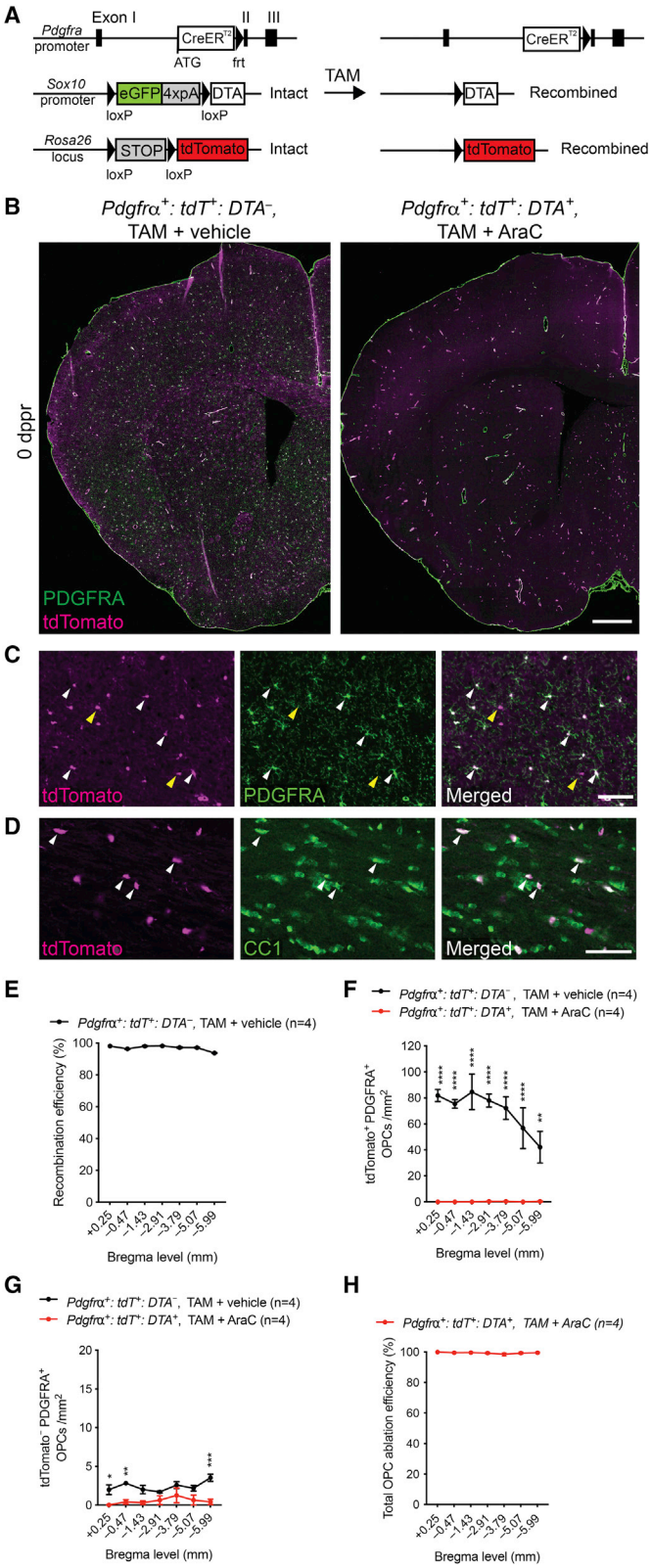


**Figure 2. Combined fate mapping and pharmacogenetic ablation enabled highly efficient and widespread OPC ablation**

(A) Schematic diagram of transgenic alleles in *Pdgfrα*$^{+}$*:tdT*$^{+}$*:DTA*$^{+}$ mice before and after TAM-induced recombination.

(B) Immunohistochemistry against PDGFRA and tdTomato in the rostral forebrain of non-ablated control (left) versus OPC-ablated (right) mice at 0 dppr. Coronal sections ~0.25 mm anterior of bregma.

(C and D) tdTomato expression in non-ablated mice (TAM + vehicle-administered *Pdgfrα*$^{+}$*:tdT*$^{+}$*:DTA*$^{-}$ mice) is observed in both PDGFRA$^{+}$ OPCs (C, white arrowheads) and in CC1$^{+}$ OLs (D, white arrowheads). tdTomato$^{+}$PDGFRA$^{-}$ cells (C, yellow arrowheads) are presumptive fate-mapped OPCs that have differentiated into OLs.

(E) Recombination efficiency of the *Ai14 tdTomato* allele across the brains of TAM + vehicle-administered *Pdgfrα*$^{+}$*:tdT*$^{+}$*:DTA*$^{-}$ mice on the basis of assessment of tdTomato expression among PDGFRA$^{+}$ OPCs. The x axis reflects rostrocaudal position relative to bregma.

(F) Cell densities of tdTomato$^{+}$ OPCs in coronal brain sections of non-ablated control versus OPC-ablated mice at 0 dppr.

(G) Densities of tdTomato$^{-}$ OPCs in entire coronal sections of non-ablated and OPC-ablated mice at 0 dppr.

(H) Percentage depletion of all PDGFRA$^{+}$ OPCs (tdTomato$^{+}$ or tdTomato$^{-}$) in OPC-ablated mice relative to non-ablated controls at 0 dppr.

Data represent mean ± SEM. Two-way ANOVA with Bonferroni's post hoc analysis (F and G); *p < 0.05, **p < 0.01, ***p < 0.001, and ****p < 0.0001. Scale bars, 500 μm (B), 100 μm (C), and 50 μm (D). See also Figure S2.

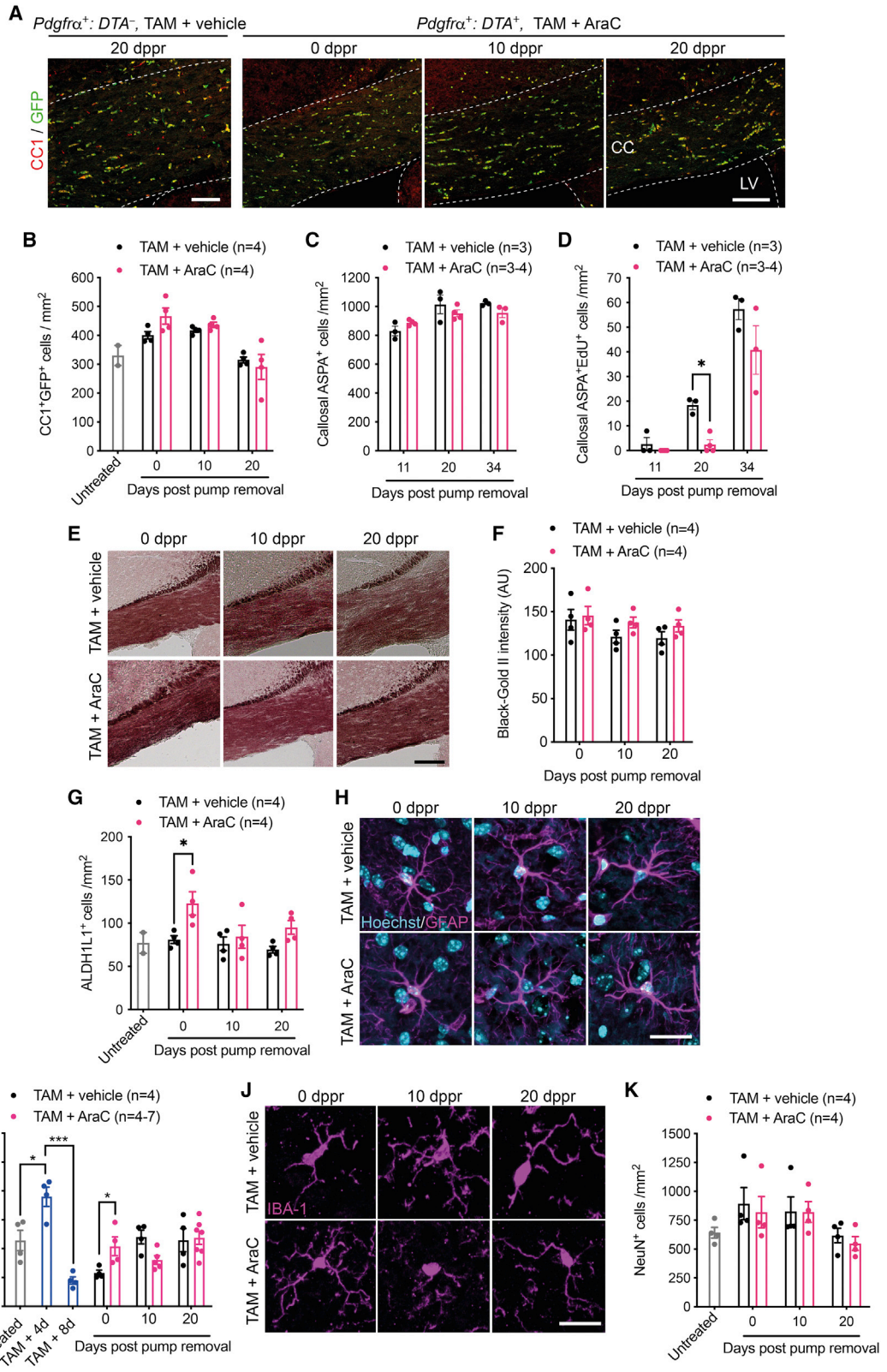


(legend on next page)

Next, we turned our examination to other glial cell types in the CNS of OPC-ablated mice. The density of ALDH1L1$^+$ astrocytes was elevated at 0 dppr in *Pdgfrα*$^+$*:DTA*$^+$ mice administered TAM + AraC and returned to control levels by 10 dppr (Figure 3G). The transient increase in astrocyte density was not accompanied by any notable change in the expression of the intermediate filament protein GFAP, a marker of astrocyte activation (Figure 3H). Similarly, the morphology of GFAP$^+$ astrocytes was equivalent in OPC-ablated and non-ablated controls, although soma size and the number and length of processes increased marginally in both groups with time post-infusion (Figures S3D–S3G).

In terms of microglial response, we observed a transient increase in the density of Iba1$^+$ microglia in *Pdgfrα*$^+$*:DTA*$^+$ mice 4 days after final TAM administration and at the end of AraC infusion (0 dppr) compared with non-ablated controls (0 dppr) which normalized by 20 dppr (Figure 3I). Morphological analysis of Iba1$^+$ microglia revealed that OPC-ablated mice exhibited changes in process complexity and somal area over time. At 0 dppr, microglia exhibited an increase in the number of secondary processes, reflective of a more active (hyper-ramified) state. Conversely, by 10 dppr, there was a significant reduction in both primary and secondary processes, as well as process length, suggesting the presence of ameboid or dystrophic microglia (Figures 3J and S3H–S3K). These morphological changes were not associated with any significant shifts in the percentage of microglia that expressed the M1- or M2-associated markers CD16/CD32 or CD206, respectively (Figures S3L and S3M), although we noted that the level of expression of CD16/CD32 was elevated at 0 dppr in OPC-ablated mice before subsequently declining. Together, these data suggest that OPC ablation induced a modest and transient neuroinflammatory response that had largely resolved by 20 dppr.

To assess whether extensive OPC ablation led to neuronal cell death through neuroinflammation as demonstrated in a previous study,[9] NeuN$^+$ neurons were quantified in the cerebral cortex where PDGFRA$^+$ cells remained depleted until 20 dppr. The densities of cortical neurons were comparable between groups at all time points (Figure 3K), irrespective of cortical layer (data not shown), suggesting that OPC ablation does not compromise the viability of cortical neurons.

## PDGFRA$^+$ cells started to repopulate the cerebrum from 12 dppr but did not derive from the OPC lineage

To examine the kinetics and anatomical origin of PDGFRA$^+$ cells that repopulated the cerebrum following OPC ablation, additional cohorts of TAM + AraC-administered *Pdgfrα*$^+$*:tdT*$^+$*:DTA*$^+$ mice were sacrificed at 0, 12, 18, 20, and 34 dppr. TAM + vehicle-administered *Pdgfrα*$^+$*:tdT*$^+$*:DTA*$^-$ mice served as non-ablated controls (Figure 4A). In the corpus callosum of OPC-ablated mice, we confirmed highly efficient ablation of tdTomato$^+$PDGFRA$^+$ OPCs at 0 dppr (Figure 4B). However, by 20 dppr, we observed high densities of PDGFRA$^+$ cells that did not express tdTomato, indicating that the vast majority of these cells do not derive from surviving tdTomato$^+$ OPCs (Figures 4B, S4A–S4C).

PDGFRA$^+$ cells repopulating the cerebrum first appeared at 12 dppr in a region of the corpus callosum adjacent to the V-SVZ. Unlike PDGFRA$^+$ cells found in the corpus callosum of non-ablated controls, those in OPC-depleted mice co-expressed Nestin, an intermediate filament protein normally expressed by cells in the V-SVZ (Figure 4C). Newly generated PDGFRA$^+$NG2$^+$ cells in OPC-depleted mice also expressed GFP, indicating that the *Sox10-DTA* allele in these cells was in a non-recombined state, indicating that they do not derive from recombined OPCs (Figure S4D). In addition, repopulating PDGFRA$^+$ cells were EdU$^+$, indicating that they were born after AraC infusion (data not shown) and many possessed a unipolar or bipolar morphology consistent with migratory activity.[27]

The density of PDGFRA$^+$ cells in the rostral cerebrum of OPC-depleted mice returned to levels similar to that of non-ablated controls in a spatiotemporally defined manner, normalizing first in the region of the corpus callosum adjacent to the V-SVZ at 12 dppr (Figure 5B), followed by the midline corpus callosum at 18 dppr (Figure 5C), and later in the cerebral cortex at 20 dppr (Figure 5D). Other regions of the rostral cerebrum of OPC-depleted mice exhibited different latencies for PDGFRA$^+$ cell density to return to control levels (Figures 5E–5H). Overall, the mean density of PDGFRA$^+$ cells in the rostral cerebrum returned to levels similar to that of non-ablated controls by 20 dppr whereas caudal regions of the cerebrum remained deficient at the same time point (Figure S2F).

**Figure 3. Effect of OPC ablation on other neural cell types**

(A) Immunolabeling of GFP and CC1 on coronal sections of the rostral corpus callosum of ablated and non-ablated control mice.

(B) Mean densities of CC1$^+$GFP$^+$ cells in the rostral forebrain (gray and white matter combined). OPC ablation did not change mature OL density at the assessed time points.

(C) Densities of ASPA$^+$ OLs in the corpus callosum remained similar in OPC-ablated versus control mice.

(D) Generation of newborn OLs (ASPA$^+$EdU$^+$ cells) after infusion was transiently reduced in OPC-ablated mice. Two-way ANOVA revealed overall effects of time ($p < 0.0001$) and treatment ($p < 0.01$).

(E) Black-Gold II-stained coronal sections of the rostral corpus callosum of vehicle- or AraC-infused mice at 0, 10, and 20 dppr.

(F) Mean Black-Gold II intensity across the entire corpus callosum.

(G) Analysis of ALDH1L1$^+$ astrocyte density in the rostral forebrain revealed an overall effect of OPC ablation ($p = 0.0038$) and a significant increase in the number of activated astrocytes was observed at the end of AraC infusion (*$p = 0.0153$).

(H) GFAP immunohistochemistry revealed minimal effect of OPC ablation on astrocyte morphology in the cerebral cortex.

(I) Densities of Iba1$^+$ cells in the rostral corpus callosum of *Pdgfrα*$^+$*:DTA*$^+$ mice that received no treatment (gray bar), TAM alone (blue bars), or either TAM + vehicle (black bars) or TAM + AraC (magenta bars) and were assessed at 0, 10 or 20 dppr.

(J) Iba1 immunohistochemistry revealed that OPC ablation transiently reduced microglial process complexity in the cerebral cortex.

(K) Densities of NeuN$^+$ cells in the rostral cerebral cortex revealed no effect of OPC ablation on cortical neuron density.

Data represent mean ± SEM. Unpaired two-tailed Student's t test (I) and two-way ANOVA with Sidak's multiple-comparisons test (B–D, F, G, and K); *$p < 0.05$ and ***$p < 0.001$. CC, corpus callosum; LV, lateral ventricle. Scale bars, 200 μm (A), 150 μm (E), 25 μm (H), and 20 μm (J). See also Figure S3.

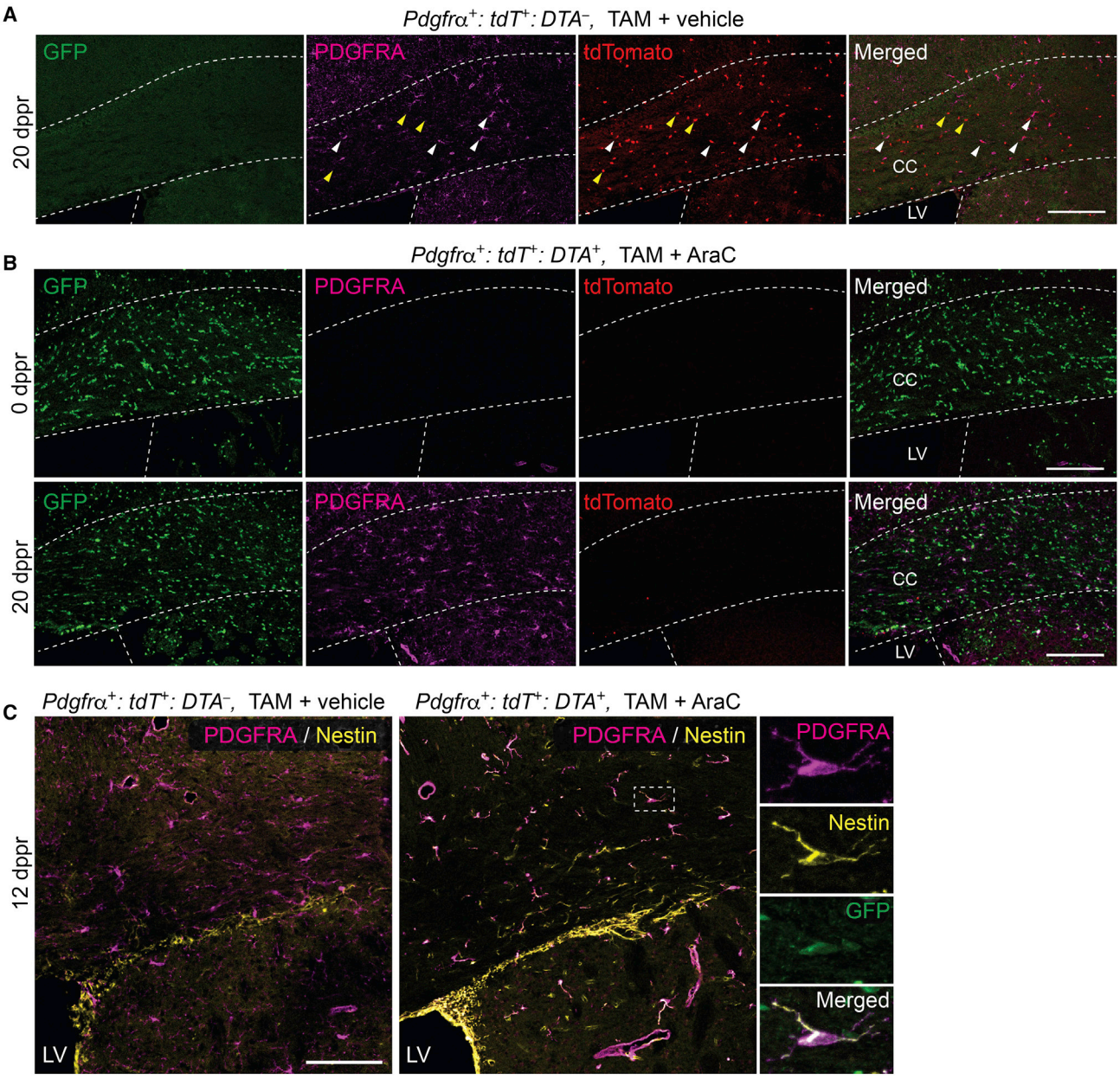


**Figure 4. PDGFRA$^+$ cells that repopulate the corpus callosum following OPC ablation do not derive from non-ablated fate-mapped OPCs**

(A and B) Immunohistochemical detection of GFP$^+$, PDGFRA$^+$, and tdTomato$^+$ cells in coronal sections of non-ablated mice at 20 dppr versus OPC-ablated mice at 0 and 20 dppr. In vehicle-infused controls the vast majority of PDGFRA$^+$ OPCs co-express tdTomato (white arrowheads). tdTomato$^+$PDGFRA$^-$ cells (yellow arrowheads) are presumptive fate-mapped OPCs that have differentiated into OLs following TAM (A).

(C) Virtually all PDGFRA$^+$ cells in the corpus callosum proximal to the V-SVZ expressed the NPC marker Nestin at the initial stage of regeneration at 12 dppr of AraC. High magnification of the boxed region reveals a GFP$^+$PDGFRA$^+$ cell expressing Nestin.

CC, corpus callosum; LV, lateral ventricle. Scale bars, 40 μm (A and B) and 100 μm (C). See also Figure S4.

Collectively these data demonstrate that ablation of 98.6% ± 0.4% of OPCs was followed by a late onset regenerative response resulting in the repopulation of PDGFRA$^+$ cells. The finding that the vast majority of repopulating PDGFRA$^+$ cells in the cerebrum were tdTomato$^-$ and GFP$^+$ is inconsistent with the notion that PDGFRA$^+$ cells arise through the proliferative expansion of surviving OPCs. Rather, the spatiotemporal pattern of PDGFRA$^+$ cell regeneration, emerging first in a region of the corpus callosum adjacent to the V-SVZ, whilst co-expressing the V-SVZ marker Nestin, raised the possibility that NPCs within the V-SVZ could be the primary source of PDGFRA$^+$ cells that re-populated this region of the brain following OPC ablation.

CellPress
OPEN ACCESS

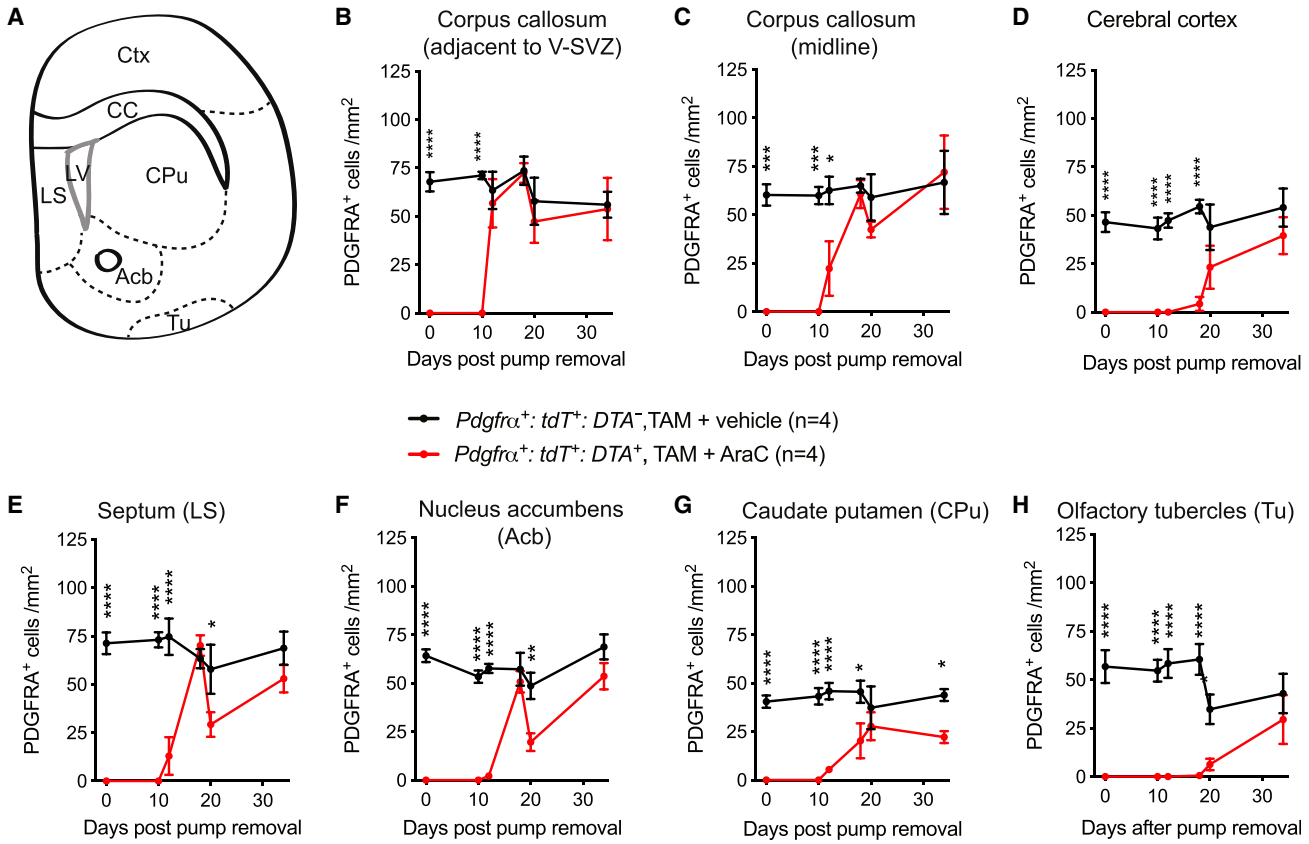


**Figure 5. Spatiotemporal profile of repopulation of newly generated PDGFRA$^+$ cells in the anterior forebrain of OPC-depleted mice**

(A) Schematic diagram depicting various brain regions of the rostral forebrain within which PDGFRA$^+$ cell densities were quantitated.

(B–H) Densities of PDGFRA$^+$ cells in various forebrain regions from 0–34 dppr revealed distinct spatiotemporal patterns of regeneration of PDGFRA$^+$ cells (n = 4 mice/group; mean ± SEM; *p < 0.05, **p < 0.01, ***p < 0.001, and ****p < 0.0001, two-way ANOVA with Bonferroni's post hoc analysis).

## Regeneration of V-SVZ-derived NPCs after AraC infusion

To investigate whether NPCs in the V-SVZ could serve as a reservoir to regenerate PDGFRA$^+$ cells, we examined the response of NPCs to pharmacogenetic ablation of OPCs. A 6-day infusion of 2% AraC onto the surface of the brain was previously demonstrated to eliminate rapidly dividing cells in the V-SVZ.[28] The subsequent activation and proliferation of quiescent neural stem cells in the V-SVZ resulted in complete regeneration of the neurogenic niche including transit-amplifying cells and neuroblasts within 10 days after AraC withdrawal.[29] To assess the regeneration of NPCs in TAM + AraC-administered *Pdgfrα$^+$:DTA$^+$* mouse brains, mice were given EdU via their drinking water beginning immediately after pump removal and continuing until they were perfused 10 days later (Figure 1H). Compared with control mice, DCX$^+$ neuroblasts were virtually absent from the V-SVZ of AraC-infused mice at 0 dppr (Figure 6A). At 10 dppr, the number of DCX$^+$ cells in the V-SVZ of AraC-treated animals was similar to that of vehicle-treated controls (Figures 6A and 6B). In addition, these DCX$^+$ cells were positive for EdU (Figure 6C), indicating that they were born after AraC infusion. We conclude that the AraC infusion ablated rapidly dividing NPCs in the V-SVZ but these cells were completely regenerated by 10 dppr.

## V-SVZ-derived NPCs contributed to the regeneration of PDGFRA$^+$ cells in the cerebrum after OPC ablation

Our earlier examination of OPC-ablated mice at 12 dppr had revealed that callosal PDGFRA$^+$ cells adjacent to the V-SVZ co-expressed Nestin, a marker of NPCs in the V-SVZ, whereas callosal OPCs in the vehicle-infused controls did not (Figure 4C). We posited that repopulating PDGFRA$^+$ cells could derive from NPCs located within the V-SVZ. In support of this possibility, we found that in the corpus callosum of OPC-ablated mice examined at 20 dppr, PDGFRA$^+$NG2$^+$ cells co-expressed GFP indicating that the *Sox10-GFP* allele was in a non-recombined state (Figure S4D). We also found that PDGFRA$^+$NG2$^+$ cells in the dorsolateral corner as well as in the dorsal and lateral walls of the V-SVZ co-labeled with EdU, which was provided to the mice following AraC infusion (data not shown).

To confirm that NPCs generate PDGFRA$^+$ cells that migrate into the cerebrum following OPC ablation, we developed a Dre recombinase-based viral approach for genetic fate mapping of V-SVZ-derived NPCs (Figures S5A–S5D). Two weeks before ablating OPCs, we injected *Pdgfrα$^+$:tdT$^+$:DTA$^+$* mice

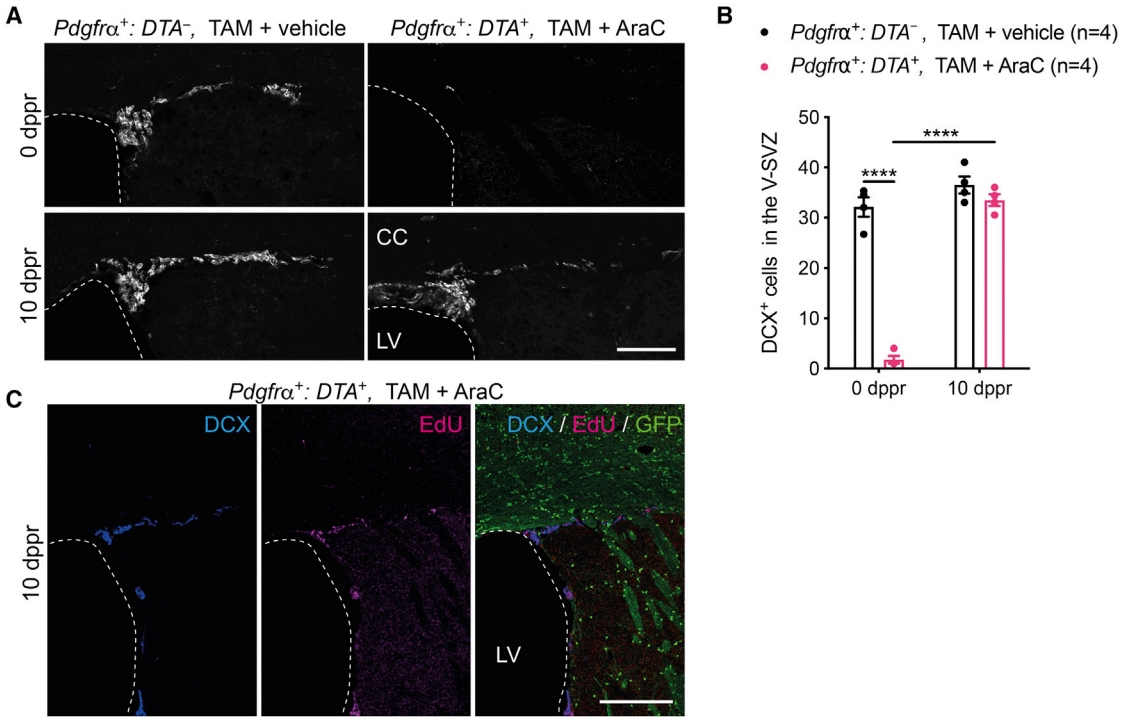


**Figure 6. AraC infusion resulted in the transient depletion of neuroblasts in the V-SVZ followed by their complete regeneration within 10 dppr**

(A) Expression of the neuroblast marker doublecortin (DCX) in the V-SVZ of non-ablated control and OPC-ablated mice assessed at 0 or 10 dppr.

(B) Densities of DCX$^+$ cells in the V-SVZ of non-ablated control and OPC-ablated mice assessed at 0 or 10 dppr (n=4 mice/group; mean ± SEM; ****$p < 0.0001$, two-way ANOVA with Bonferroni's post hoc analysis).

(C) Coronal sections of the V-SVZ immunolabeled with antibodies against GFP and DCX, and stained for EdU. EdU$^+$ neuroblasts defined by co-expression of DCX were restricted to the V-SVZ.

CC, corpus callosum; LV, lateral ventricle. Scale bars, 100 μm (A) and 200 μm (C).

with lentiviruses to transduce NPCs in the V-SVZ (Figure 7A). This resulted in the expression of a Myc-tagged membrane-targeted mKate2 fluorescent reporter protein by a subset of cells in the V-SVZ (Figures S5E–S5I). At 20 dppr, we detected mKate2 in a subpopulation of newly generated PDGFRA$^+$ cells in the corpus callosum, indicating that they had derived from NPCs (Figures 7B and 7C). We corroborated the V-SVZ origin of newly generated PDGFRA$^+$ cells by simultaneous ablation of both parenchymal OPCs and oligodendrogenic NPCs using *Nestin-CreER$^{T2+/-}$; Pdgfrα-CreER$^{T2+/-}$; Sox10-DTA$^{+/-}$* transgenic mice (denoted hereafter as *Nestin$^+$:Pdgfra$^+$:DTA$^+$* mice) (Figure 7D). The persistent absence of PDGFRA$^+$ cells in the cerebrum of parenchymal OPC and oligodendrogenic NPC co-ablated mice at 20 dppr after AraC withdrawal indicates that regenerating PDGFRA$^+$ cells in the dorsal cerebrum of OPC-ablated mice derive principally from Nestin-expressing NPCs residing in the V-SVZ (Figures 7E, 7F, and S5J). Of note, *Nestin$^+$:Pdgfra$^+$:DTA$^+$* mice exhibited hydrocephalus, which we believe reflects a degree of TAM-independent recombination in SOX10$^+$Nestin$^+$ neural crest cells during development (see STAR Methods, Experimental model and subject details, Animals). Despite evidence of hydrocephalus, we observed a similar density of neurogenic NPCs expressing DCX in the lateral walls and dorsolateral corner of the V-SVZ of TAM + AraC-administered *Nestin$^+$:Pdgfra$^+$:DTA$^+$* mice compared with non-ablated controls (Figures S5L and S5M). Thus, although neuroblast production persists in TAM + AraC-administered *Nestin$^+$:Pdgfra$^+$:DTA$^+$* mice, PDGFRA$^+$ cells are not viable. Collectively, these data indicate that PDGFRA$^+$ cells that repopulate the dorsal cerebrum of OPC-depleted mice beginning 12 dppr arise principally from oligodendrogenic NPCs residing in the V-SVZ.

## DISCUSSION

The development of methods to conditionally ablate OPCs in the adult mouse CNS provides a powerful experimental paradigm to explore their function. Although several approaches have been described,[5–10] the techniques established to date have not allowed the complete depletion of OPCs throughout the brain. Without complete OPC ablation, surviving OPCs enter the cell cycle and rapidly regenerate their population, complicating the interpretation of results. To avert rapid regeneration by surviving OPCs, we have developed a pharmacogenetic approach that allows high-efficiency ablation of OPCs throughout the brain. This approach consists of genetic elements permitting TAM-dependent induction of DTA expression exclusively in OPCs followed by a pharmacological intervention to prevent repopulation by OPCs that avert genetic targeting. Genetic control of OPC ablation is achieved by crossing the *Pdgfra-CreER$^{T2}$* and

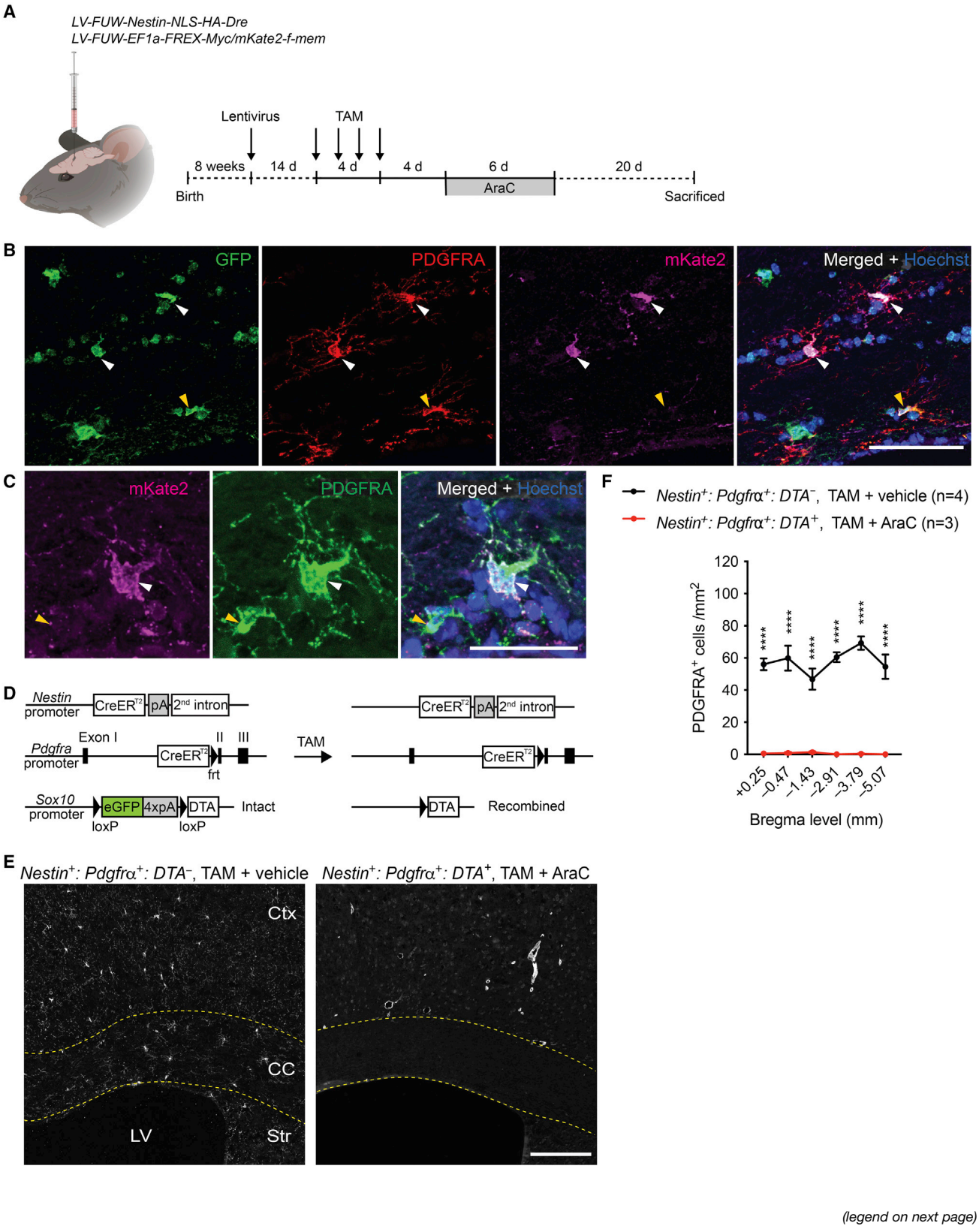


(legend on next page)

*Sox10-lox-GFP-STOP-lox-DTA* transgenic mouse lines. Double transgenic mice enable highly specific ablation of OPCs at a prescribed time point due to the dependence of DTA expression upon three levels of regulation: (1) activity of the *Pdgfra* promoter, (2) activity of the oligodendroglial-specific *Sox10* promoter, and (3) temporal control provided by TAM-dependent regulation of $CreER^{T2}$ activity. However, delivery of TAM alone to *Pdgfrα*$^{+}$*:DTA*$^{+}$ mice was insufficient for complete or durable OPC ablation, because of the rapid proliferation of residual surviving OPCs. As cumulative toxicity precludes delivery of TAM beyond 4 days, following TAM delivery, mice were infused intracisternally with the anti-mitotic drug AraC to prevent OPCs that escape genetic targeting from re-entering the cell cycle and repopulating the brain. In isolation, intracisternal infusion of AraC to wild-type mice did not reduce OPC density, consistent with the fact that only a fraction of OPCs in the healthy adult CNS are dividing at a given time and the homeostatic control mechanisms that maintain OPC density when OPCs are sparsely depleted.[6] However, the combined use of both genetic and pharmacological approaches eliminated 98.6% ± 0.4% of all OPCs throughout the brain without causing any overt adverse effects on the health of animals.

The combined pharmacogenetic approach that we have developed to target OPCs is anticipated to result in the death of cells expressing both PDGFRA and SOX10 and mitotic cells exposed to AraC. By examining the densities of various non-OPC cell types in the brains of OPC-ablated mice, our data suggest that although OPCs, as well as committed oligodendrocyte progenitors (PDGFRA$^{-}$GPR17$^{+}$) and DCX$^{+}$ cells in the V-SVZ, are depleted, the density of mature OLs and neurons remains unchanged. Significantly however, the ablation of OPCs is anticipated to trigger a broad range of direct and indirect effects upon other neural cell types that are not necessarily reflected by a change in cell density. For instance, the activation of microglia to facilitate phagocytosis of cellular debris of OPCs undergoing cell death is expected.[30] Indeed, we identified an initial increase and subsequent decrease in the density of microglia over the course of OPC ablation and subsequent regeneration. We also observed changes in microglial phenotype suggesting that OPC ablation alters their activation status. Given these observations, the effect that changes in microglial density and activation status have upon behavioral, cellular and molecular readouts should be taken into consideration in the future application of the model. One approach to address the role that microglia exert in this model would be to deplete microglia via inhibition of the colony-stimulating factor 1 receptor,[31] in the context of OPC ablation, to discern the immune-mediated effects of OPC ablation from primary effects caused by depletion of OPCs. The effects of OPC ablation on other neural cell types, such as endothelial cells, remain to be determined.

Despite the highly efficient ablation of OPCs throughout the brain, PDGFRA$^{+}$NG2$^{+}$ cells were eventually regenerated, beginning from around 12 dppr. In this context, it is important to note that AraC infusion also ablated almost all DCX$^{+}$ neuroblasts in the V-SVZ before their return to normal density by 10 dppr. The transient depletion of DCX$^{+}$ cells in the V-SVZ is consistent with previous reports demonstrating that AraC-mediated elimination of rapidly dividing transit-amplifying cells and neuroblasts in the V-SVZ activates quiescent neural stem cells to re-enter the cell cycle, leading to complete regeneration of neuroblasts in the V-SVZ within 10 days following AraC withdrawal.[28,29] The kinetics of neuroblast regeneration in the V-SVZ aligned closely with the spatiotemporal pattern of PDGFRA$^{+}$NG2$^{+}$ cell regeneration in the cerebrum. First, we noted that recombined (tdTomato$^{+}$) OPCs did not contribute to the regeneration of PDGFRA$^{+}$ cells. Rather, we showed that non-recombined (GFP$^{+}$) PDGFRA$^{+}$ cells arose first in the vicinity of the V-SVZ and expressed Nestin, a known V-SVZ marker, shortly after DCX$^{+}$ cell density returned to control levels after ablation. This observation could be explained by two distinct possibilities. Our *a priori* view was that this reflected recruitment of oligodendrogenic NPCs from the V-SVZ that maintain their expression of Nestin for some time after they migrate out of the V-SVZ, given the known capacity of the V-SVZ to generate PDGFRA$^{+}$NG2$^{+}$ cells in health and disease.[32,33] An alternate possibility is that Nestin$^{+}$GFP$^{+}$PDGFRA$^{+}$ cells observed at 12 dppr reflect non-recombined OPCs that survive pharmacogenetic ablation and transiently upregulate Nestin in response to neuroinflammatory cues, as has been described for astrocytes under ischemic conditions.[34,35] Countering this alternate possibility, we found that lentiviral-mediated labeling of Nestin-expressing cells in the V-SVZ prior to OPC ablation allowed us to identify mKate2$^{+}$PDGFRA$^{+}$ cells in the corpus callosum following OPC ablation, providing additional evidence to support the V-SVZ origin of repopulating PDGFRA$^{+}$ cells in the cerebrum. Although this experiment demonstrates that NPCs lining the lateral ventricles can give rise to PDGFRA$^{+}$ cells during the regenerative phase that follows OPC ablation, the limited efficiency of this viral labeling approach cannot account for all PDGFRA$^{+}$ cells that are regenerated in the cerebrum. We addressed this issue by adopting a co-ablation strategy that directs Sox10-dependent DTA

**Figure 7. V-SVZ-derived NPCs were responsible for the regeneration of new PDGFRA$^{+}$ cells in the anterior/dorsal forebrain after OPC ablation**

(A) Experimental timeline for lentiviral fate mapping of V-SVZ-derived NPCs. Diagram created using BioRender.

(B and C) In TAM + AraC-administered *Pdgfrα*$^{+}$*:tdT*$^{+}$*:DTA*$^{+}$ mice assessed at 20 dppr, immunostaining with antibodies against PDGFRA, GFP, and mKate2 revealed lentivirally transduced newly generated PDGFRA$^{+}$ cells (white arrowheads) expressing membrane-targeted mKate2 in the corpus callosum proximal to the V-SVZ. Non-transduced PDGFRA$^{+}$ cells are indicated with yellow arrowheads.

(D) Schematic diagram of transgenic alleles in *Nestin*$^{+}$*:Pdgfrα*$^{+}$*:DTA*$^{+}$ mice before and after TAM-induced recombination.

(E) Immunolabeling of PDGFRA in the rostral cerebrum of non-ablated controls (*Nestin*$^{+}$*:Pdgfrα*$^{+}$*:DTA*$^{-}$, TAM + vehicle mice) and in parenchymal OPC and oligodendrogenic NPC co-ablated mice (*Nestin*$^{+}$*:Pdgfrα*$^{+}$*:DTA*$^{+}$, TAM + AraC) at 20 dppr.

(F) Densities of PDGFRA$^{+}$ cells in the cerebrum of non-ablated controls and in parenchymal OPC and oligodendrogenic NPC co-ablated mice at 20 dppr (n = 3–4 mice/group; mean ± SEM; ****p < 0.0001, two-way ANOVA with Bonferroni's post hoc analysis).

Ctx, cortex; CC, corpus callosum; LV, lateral ventricle; Str, striatum. Scale bars, 60 μm (B), 30 μm (C), and 100 μm (E). See also Figure S5.

expression to both the NPC and OPC lineages. Using this approach, we found that the co-ablation of both parenchymal OPCs and oligodendrogenic NPCs resulted in failure to regenerate PDGFRA$^+$ cells in the dorsal cerebrum, providing robust evidence that repopulating PDGFRA$^+$ cells in the cerebrum derive from NPCs.

A potential caveat of the co-ablation strategy that warrants consideration is the fidelity with which the *Nestin-CreER$^{T2}$* driver is restricted to NPCs. Let us first consider the possibility that the PDGFRA$^+$ cells that we observe during early repopulation reflect surviving OPCs that express Nestin ectopically under inflammatory conditions rather than cells of NPC origin. If this were the case, ablation of Nestin-expressing OPCs that survive pharmacogenetic ablation in *Nestin$^+$:Pdgfra$^+$:DTA$^+$* mice would require 100% of these putative Nestin-expressing OPCs to exhibit TAM-independent recombination of the *Sox10-DTA* allele. We were able to exclude this possibility by demonstrating that TAM-independent recombination in NPCs with a history of up to 10 weeks of postnatal Nestin expression occurs with a frequency of less than 1% (Figure S5P). Given these findings, the most parsimonious explanation is that following TAM gavage in *Nestin$^+$:Pdgfr$\alpha^+$:DTA$^+$* mice, the recombined *Sox10-DTA* allele starts to be expressed by NPCs upon their specification to an oligodendroglial fate, which induces DTA-mediated apoptosis of oligodendrogenic NPCs.

Our findings expand on previous work demonstrating that NPCs originating in the V-SVZ give rise to oligodendrogenic progenitors, both under normal physiological conditions and in response to demyelination of proximal white matter tracts.[32,33,36,37] Another study, in which mice undergo global *Pdgfra* inactivation resulting in OPC depletion, suggested that repopulation of OPCs occurred by expansion of OPCs originating from immature Nestin-expressing cells activated in the meninges and brain parenchyma and from OPCs that escape *Pdgfra* inactivation.[10] However, our data do not support a meningeal origin for newly generated PDGFRA$^+$NG2$^+$ cells (Figures S5N and S5O).

Collectively, our mouse model of conditional OPC ablation provides a long-sought-after methodology to eliminate OPCs in the adult mouse CNS. The model now provides the opportunity to explore the role that OPCs play in CNS homeostasis by probing the consequences of their ablation through various approaches including, but not limited to, single-cell RNA sequencing and proteomic analysis to identify the transcriptional and post-translational changes of OPC-ablated versus non-ablated mice.

### Limitations of the study

The strength of our finding that OPC-deficient mice have no OPCs in their cerebrum at 0 dppr is limited by the tissue sampling strategy that we adopted. As we did not analyze every single section from each mouse brain, or collect sections from the entire rostral and caudal extent of the cerebrum, we cannot exclude the possibility that there could be some OPCs in sections of the cerebrum that were not examined. We conducted a probability analysis to predict the number of OPCs that could theoretically be present within the region of the cerebrum from which sections were sampled (see STAR Methods, Probability calculations). We calculated an even-chance probability that ~97.2% of all sections of the cerebrum are devoid of OPCs (Figure S1E). We estimate on this basis that each OPC-deficient mouse is likely to have fewer than about 15 OPCs in the cerebrum within the region of interest (+0.25 to −5.07 mm A/P relative to bregma). Further analysis of OPC-deficient mice, including the more rostral and caudal extents of the cerebrum, would be required to determine the absolute number of OPCs in the cerebrum that escape ablation. Consequently, we cannot exclude the possibility that there are some OPCs in the cerebrum that escape ablation and that subsequently contribute to the regeneration of cerebral PDGFRA$^+$ cells following OPC ablation, in addition to the large numbers of PDGFRA$^+$ cells that derive from oligodendrogenic NPCs residing in the V-SVZ.

Although we were able to identify a V-SVZ origin for the majority of repopulating PDGFRA$^+$ cells in the cerebrum, we are unable to clearly identify the origin of PDGFRA$^+$ cells that repopulated the brainstem. Although most PDGFRA$^+$ cells in the brainstem were tdTomato$^-$, there were many that were tdTomato$^+$ (Figure S2G). An even higher fraction of repopulating PDGFRA$^+$ cells was found to express tdTomato in the spinal cord and optic nerve, areas that also exhibited robust OPC depletion (Figures S4E–S4H). Repopulating tdTomato$^+$PDGFRA$^+$ cells in the brainstem co-expressed GFP, indicating that they likely originate by clonal expansion of pre-existing OPCs in which the *Ai14 tdTomato* but not the *Sox10-DTA* allele had recombined. In addition, the regeneration of tdTomato$^-$ PDGFRA$^+$ cells in the brainstem could reflect repopulation by OPCs that escape recombination of both the *Ai14 tdTomato* and *Sox10-DTA* alleles and survive AraC infusion. Alternatively, it is also plausible that repopulating tdTomato$^-$ PDGFRA$^+$ cells could arise from immature progenitors residing within alternate stem cell niches located within the brainstem. An oligodendrogenic niche has recently been described in the median eminence of the hypothalamus bordering the third ventricle.[38] Other putative stem cell niches include the ependymal and subependymal zones of the third and fourth ventricles.[39] Notably, we identified high densities of PDGFRA$^+$ cells around the aqueduct (Figure S2D) and the fourth ventricle (data not shown) at 10 dppr. It thus seems likely that the homeostatic regeneration of PDGFRA$^+$NG2$^+$ cells following OPC depletion is mediated by distinct populations of progenitors in the cerebrum and brainstem.

## STAR★METHODS

Detailed methods are provided in the online version of this paper and include the following:

- KEY RESOURCES TABLE
- RESOURCE AVAILABILITY
  - Lead contact
  - Materials availability
  - Data and code availability
- EXPERIMENTAL MODEL AND SUBJECT DETAILS
  - Animals
- METHOD DETAILS
  - Timelines of experimental interventions for high-efficiency OPC ablation
  - TAM gavage

- EdU administration
- Preparation of AraC for intracisternal infusions
- Surgical implantation of osmotic minipumps
- Surgical removal of osmotic minipumps
- Generation of lentiviral vectors
- *In vitro* validation of lentiviral vectors
- Lentivirus production
- Intraventricular injection of lentiviral vectors
- Tissue processing and immunohistochemistry
- Imaging
- Image processing

● QUANTIFICATION AND STATISTICAL ANALYSIS

- Image analysis and cell quantification
- Probability calculations
- Statistical analyses

## SUPPLEMENTAL INFORMATION

Supplemental information can be found online at https://doi.org/10.1016/j.crmeth.2023.100414.

## ACKNOWLEDGMENTS

This work was supported by the Australian Research Council Special Research Initiative – Stem Cells Australia (T.D.M., T.J.K.) and was supported in part by the Intramural Research Program of the National Institute of Mental Health (NIMH). Y.L.X. received support from the Cass Foundation (8545). T.D.M. was the recipient of a Future Fellowship from the Australian Research Council (FT150100207) and received philanthropic support from Metal Manufactures Ltd. The Australian Regenerative Medicine Institute is supported by grants from the State Government of Victoria and the Australian Government. We thank Prof. Ryoichiro Kageyama (RIKEN Center for Brain Science, Japan) for generously providing the *Nestin-CreER$^{T2}$ (line 5.1)* mice. We thank Prof. Nicoletta Kessaris (University College London, UK) for generously providing the *Sox10-lox-GFP-poly(A)-lox-DTA* mice. We thank Sun Jung Kang (NIMH, National Institutes of Health [NIH]) for advice on probability calculations. We acknowledge the use of facilities within the Monash Animal Research Platform, Monash Micro Imaging Platform, Monash Histology Platform, and Micromon (Monash University).

## AUTHOR CONTRIBUTIONS

Conceptualization, Y.L.X. and T.D.M.; methodology, Y.L.X. and T.D.M.; investigation, Y.L.X., Y.O., J.P., B.H.A.C., K.M., S.M., and T.D.M; resources, W.D.R.; writing – original draft, Y.L.X. and T.D.M.; writing – review & editing, Y.L.X., W.D.R., T.J.K., and T.D.M.; supervision, T.D.M.; funding acquisition, T.D.M.

## DECLARATION OF INTERESTS

The authors declare no competing interests.

## INCLUSION AND DIVERSITY

We support inclusive, diverse, and equitable conduct of research.

Received: April 18, 2022
Revised: October 11, 2022
Accepted: January 30, 2023
Published: February 27, 2023

## REFERENCES

1. Kang, S.H., Fukaya, M., Yang, J.K., Rothstein, J.D., and Bergles, D.E. (2010). NG2+ CNS glial progenitors remain committed to the oligodendrocyte lineage in postnatal life and following neurodegeneration. Neuron *68*, 668–681. https://doi.org/10.1016/j.neuron.2010.09.009.
2. Young, K.M., Psachoulia, K., Tripathi, R.B., Dunn, S.J., Cossell, L., Attwell, D., Tohyama, K., and Richardson, W.D. (2013). Oligodendrocyte dynamics in the healthy adult CNS: evidence for myelin remodeling. Neuron *77*, 873–885. https://doi.org/10.1016/j.neuron.2013.01.006.
3. Chittajallu, R., Aguirre, A., and Gallo, V. (2004). NG2-positive cells in the mouse white and grey matter display distinct physiological properties. J. Physiol. *561*, 109–122. https://doi.org/10.1113/jphysiol.2004.074252.
4. Spitzer, S.O., Sitnikov, S., Kamen, Y., Evans, K.A., Kronenberg-Versteeg, D., Dietmann, S., de Faria, O., Jr., Agathou, S., and Káradóttir, R.T. (2019). Oligodendrocyte progenitor cells become regionally diverse and heterogeneous with age. Neuron *101*, 459–471.e5. https://doi.org/10.1016/j.neuron.2018.12.020.
5. Irvine, K.A., and Blakemore, W.F. (2007). A different regional response by mouse oligodendrocyte progenitor cells (OPCs) to high-dose X-irradiation has consequences for repopulating OPC-depleted normal tissue. Eur. J. Neurosci. *25*, 417–424. https://doi.org/10.1111/j.1460-9568.2007.05313.x.
6. Hughes, E.G., Kang, S.H., Fukaya, M., and Bergles, D.E. (2013). Oligodendrocyte progenitors balance growth with self-repulsion to achieve homeostasis in the adult brain. Nat. Neurosci. *16*, 668–676. https://doi.org/10.1038/nn.3390.
7. Robins, S.C., Villemain, A., Liu, X., Djogo, T., Kryzskaya, D., Storch, K.F., and Kokoeva, M.V. (2013). Extensive regenerative plasticity among adult NG2-glia populations is exclusively based on self-renewal. Glia *61*, 1735–1747. https://doi.org/10.1002/glia.22554.
8. Birey, F., Kloc, M., Chavali, M., Hussein, I., Wilson, M., Christoffel, D.J., Chen, T., Frohman, M.A., Robinson, J.K., Russo, S.J., et al. (2015). Genetic and stress-induced loss of NG2 glia triggers emergence of depressive-like behaviors through reduced secretion of FGF2. Neuron *88*, 941–956. https://doi.org/10.1016/j.neuron.2015.10.046.
9. Nakano, M., Tamura, Y., Yamato, M., Kume, S., Eguchi, A., Takata, K., Watanabe, Y., and Kataoka, Y. (2017). NG2 glial cells regulate neuroimmunological responses to maintain neuronal function and survival. Sci. Rep. *7*, 42041. https://doi.org/10.1038/srep42041.
10. Đặng, T.C., Ishii, Y., Nguyen, V.D., Yamamoto, S., Hamashima, T., Okuno, N., Nguyen, Q.L., Sang, Y., Ohkawa, N., Saitoh, Y., et al. (2019). Powerful homeostatic control of oligodendroglial lineage by PDGFRalpha in adult brain. Cell Rep. *27*, 1073–1089.e5. https://doi.org/10.1016/j.celrep.2019.03.084.
11. Nishiyama, A., Komitova, M., Suzuki, R., and Zhu, X. (2009). Polydendrocytes (NG2 cells): multifunctional cells with lineage plasticity. Nat. Rev. Neurosci. *10*, 9–22. https://doi.org/10.1038/nrn2495.
12. Rivers, L.E., Young, K.M., Rizzi, M., Jamen, F., Psachoulia, K., Wade, A., Kessaris, N., and Richardson, W.D. (2008). PDGFRA/NG2 glia generate myelinating oligodendrocytes and piriform projection neurons in adult mice. Nat. Neurosci. *11*, 1392–1401. https://doi.org/10.1038/nn.2220.
13. Chang, Y., She, Z.G., Sakimura, K., Roberts, A., Kucharova, K., Rowitch, D.H., and Stallcup, W.B. (2012). Ablation of NG2 proteoglycan leads to deficits in brown fat function and to adult onset obesity. PLoS One *7*, e30637. https://doi.org/10.1371/journal.pone.0030637.
14. Ziskin, J.L., Nishiyama, A., Rubio, M., Fukaya, M., and Bergles, D.E. (2007). Vesicular release of glutamate from unmyelinated axons in white matter. Nat. Neurosci. *10*, 321–330. https://doi.org/10.1038/nn1854.
15. Marques, S., Zeisel, A., Codeluppi, S., van Bruggen, D., Mendanha Falcão, A., Xiao, L., Li, H., Häring, M., Hochgerner, H., Romanov, R.A., et al. (2016). Oligodendrocyte heterogeneity in the mouse juvenile and adult central nervous system. Science *352*, 1326–1329. https://doi.org/10.1126/science.aaf6463.

16. Vanlandewijck, M., He, L., Mäe, M.A., Andrae, J., Ando, K., Del Gaudio, F., Nahar, K., Lebouvier, T., Laviña, B., Gouveia, L., et al. (2018). A molecular atlas of cell types and zonation in the brain vasculature. Nature *554*, 475–480. https://doi.org/10.1038/nature25739.

17. Zhu, L., Su, Q., Jie, X., Liu, A., Wang, H., He, B., and Jiang, H. (2016). NG2 expression in microglial cells affects the expression of neurotrophic and proinflammatory factors by regulating FAK phosphorylation. Sci. Rep. *6*, 27983. https://doi.org/10.1038/srep27983.

18. Schatteman, G.C., Morrison-Graham, K., van Koppen, A., Weston, J.A., and Bowen-Pope, D.F. (1992). Regulation and role of PDGF receptor alpha-subunit expression during embryogenesis. Development *115*, 123–131.

19. Pringle, N.P., Mudhar, H.S., Collarini, E.J., and Richardson, W.D. (1992). PDGF receptors in the rat CNS: during late neurogenesis, PDGF alpha-receptor expression appears to be restricted to glial cells of the oligodendrocyte lineage. Development *115*, 535–551.

20. Kessaris, N., Fogarty, M., Iannarelli, P., Grist, M., Wegner, M., and Richardson, W.D. (2006). Competing waves of oligodendrocytes in the forebrain and postnatal elimination of an embryonic lineage. Nat. Neurosci. *9*, 173–179. https://doi.org/10.1038/nn1620.

21. Xu, X., Cai, J., Fu, H., Wu, R., Qi, Y., Modderman, G., Liu, R., and Qiu, M. (2000). Selective expression of Nkx-2.2 transcription factor in chicken oligodendrocyte progenitors and implications for the embryonic origin of oligodendrocytes. Mol. Cell. Neurosci. *16*, 740–753. https://doi.org/10.1006/mcne.2000.0916.

22. Lu, Q.R., Yuk, D., Alberta, J.A., Zhu, Z., Pawlitzky, I., Chan, J., McMahon, A.P., Stiles, C.D., and Rowitch, D.H. (2000). Sonic hedgehog–regulated oligodendrocyte lineage genes encoding bHLH proteins in the mammalian central nervous system. Neuron *25*, 317–329. https://doi.org/10.1016/s0896-6273(00)80897-1.

23. Britsch, S., Goerich, D.E., Riethmacher, D., Peirano, R.I., Rossner, M., Nave, K.A., Birchmeier, C., and Wegner, M. (2001). The transcription factor Sox10 is a key regulator of peripheral glial development. Genes Dev. *15*, 66–78. https://doi.org/10.1101/gad.186601.

24. Eccleston, P.A., Funa, K., and Heldin, C.H. (1993). Expression of platelet-derived growth factor (PDGF) and PDGF alpha- and beta-receptors in the peripheral nervous system: an analysis of sciatic nerve and dorsal root ganglia. Dev. Biol. *155*, 459–470. https://doi.org/10.1006/dbio.1993.1044.

25. Zawadzka, M., Rivers, L.E., Fancy, S.P.J., Zhao, C., Tripathi, R., Jamen, F., Young, K., Goncharevich, A., Pohl, H., Rizzi, M., et al. (2010). CNS-resident glial progenitor/stem cells produce Schwann cells as well as oligodendrocytes during repair of CNS demyelination. Cell Stem Cell *6*, 578–590. https://doi.org/10.1016/j.stem.2010.04.002.

26. Gonsalvez, D.G., Craig, G.A., Walsh, D.M., Hughes, B.D., Wood, R.J., Yoo, S.W., Murray, S.S., and Xiao, J. (2019). The dynamics of oligodendrocyte generation: how distinct is the mouse from the human?. Preprint at bioRxiv. https://doi.org/10.1101/2019.12.23.887174.

27. Tsai, H.H., Macklin, W.B., and Miller, R.H. (2009). Distinct modes of migration position oligodendrocyte precursors for localized cell division in the developing spinal cord. J. Neurosci. Res. *87*, 3320–3330. https://doi.org/10.1002/jnr.22058.

28. Doetsch, F., Caillé, I., Lim, D.A., García-Verdugo, J.M., and Alvarez-Buylla, A. (1999). Subventricular zone astrocytes are neural stem cells in the adult mammalian brain. Cell *97*, 703–716. https://doi.org/10.1016/s0092-8674(00)80783-7.

29. Doetsch, F., García-Verdugo, J.M., and Alvarez-Buylla, A. (1999). Regeneration of a germinal layer in the adult mammalian brain. Proc. Natl. Acad. Sci. USA *96*, 11619–11624. https://doi.org/10.1073/pnas.96.20.11619.

30. Márquez-Ropero, M., Benito, E., Plaza-Zabala, A., and Sierra, A. (2020). Microglial corpse clearance: lessons from macrophages. Front. Immunol. *11*, 506. https://doi.org/10.3389/fimmu.2020.00506.

31. Green, K.N., Crapser, J.D., and Hohsfield, L.A. (2020). To kill a microglia: a case for CSF1R inhibitors. Trends Immunol. *41*, 771–784. https://doi.org/10.1016/j.it.2020.07.001.

32. Menn, B., Garcia-Verdugo, J.M., Yaschine, C., Gonzalez-Perez, O., Rowitch, D., and Alvarez-Buylla, A. (2006). Origin of oligodendrocytes in the subventricular zone of the adult brain. J. Neurosci. *26*, 7907–7918. https://doi.org/10.1523/JNEUROSCI.1299-06.2006.

33. Xing, Y.L., Röth, P.T., Stratton, J.A.S., Chuang, B.H.A., Danne, J., Ellis, S.L., Ng, S.W., Kilpatrick, T.J., and Merson, T.D. (2014). Adult neural precursor cells from the subventricular zone contribute significantly to oligodendrocyte regeneration and remyelination. J. Neurosci. *34*, 14128–14146. https://doi.org/10.1523/JNEUROSCI.3491-13.2014.

34. Lin, R.C., Matesic, D.F., Marvin, M., McKay, R.D., and Brüstle, O. (1995). Re-expression of the intermediate filament nestin in reactive astrocytes. Neurobiol. Dis. *2*, 79–85. https://doi.org/10.1006/nbdi.1995.0008.

35. Duggal, N., Schmidt-Kastner, R., and Hakim, A.M. (1997). Nestin expression in reactive astrocytes following focal cerebral ischemia in rats. Brain Res. *768*, 1–9. https://doi.org/10.1016/s0006-8993(97)00588-x.

36. Brousse, B., Magalon, K., Durbec, P., and Cayre, M. (2015). Region and dynamic specificities of adult neural stem cells and oligodendrocyte precursors in myelin regeneration in the mouse brain. Biol. Open *4*, 980–992. https://doi.org/10.1242/bio.012773.

37. Samanta, J., Grund, E.M., Silva, H.M., Lafaille, J.J., Fishell, G., and Salzer, J.L. (2015). Inhibition of Gli1 mobilizes endogenous neural stem cells for remyelination. Nature *526*, 448–452. https://doi.org/10.1038/nature14957.

38. Zilkha-Falb, R., Kaushansky, N., and Ben-Nun, A. (2020). The median eminence, A new oligodendrogenic niche in the adult mouse brain. Stem Cell Rep. *14*, 1076–1092. https://doi.org/10.1016/j.stemcr.2020.04.005.

39. Lin, R., and Iacovitti, L. (2015). Classic and novel stem cell niches in brain homeostasis and repair. Brain Res. *1628*, 327–342. https://doi.org/10.1016/j.brainres.2015.04.029.

40. Imayoshi, I., Ohtsuka, T., Metzger, D., Chambon, P., and Kageyama, R. (2006). Temporal regulation of Cre recombinase activity in neural stem cells. Genesis *44*, 233–238. https://doi.org/10.1002/dvg.20212.

41. Plummer, N.W., Ungewitter, E.K., Smith, K.G., Yao, H.H.C., and Jensen, P. (2017). A new mouse line for cell ablation by diphtheria toxin subunit A controlled by a Cre-dependent FLEx switch. Genesis *55*, e23067. https://doi.org/10.1002/dvg.23067.

42. Zhu, S., Liu, W., Ding, H.F., Cui, H., and Yang, L. (2019). BMP4 and Neuregulin regulate the direction of mouse neural crest cell differentiation. Exp. Ther. Med. *17*, 3883–3890. https://doi.org/10.3892/etm.2019.7439.

43. Rodríguez, E.M., Guerra, M.M., Vío, K., González, C., Ortloff, A., Bátiz, L.F., Rodríguez, S., Jara, M.C., Muñoz, R.I., Ortega, E., et al. (2012). A cell junction pathology of neural stem cells leads to abnormal neurogenesis and hydrocephalus. Biol. Res. *45*, 231–242. https://doi.org/10.4067/S0716-97602012000300005.

44. Lin, J.R., Fallahi-Sichani, M., Chen, J.Y., and Sorger, P.K. (2016). Cyclic immunofluorescence (CycIF), A highly multiplexed method for single-cell imaging. Curr. Protoc. Chem. Biol. *8*, 251–264. https://doi.org/10.1002/cpch.14.

## STAR★METHODS

### KEY RESOURCES TABLE

| REAGENT or RESOURCE | SOURCE | IDENTIFIER |
|---|---|---|
| **Antibodies** | | |
| Rabbit polyclonal anti-ALDH1L1 | Abcam | Cat# ab87117; RRID: AB_10712968 |
| Rabbit polyclonal anti-ASPA | GeneTex | Cat# GTX113389; RRID: AB_2036283 |
| Mouse monoclonal anti-CC-1 | Millipore | Cat# OP80; RRID: AB_2057371 |
| Rat monoclonal anti-CD16/CD32, clone 2.4G2 | BD Biosciences | Cat# 553142; RRID: AB_394657 |
| Rabbit polyclonal anti-CD206 | Abcam | Cat# ab64693; RRID: AB_1523910 |
| Goat polyclonal anti-DCX | Santa Cruz Biotechnology | Cat# sc-8066; RRID: AB_2088494 |
| Mouse monoclonal anti-FoxJ1, clone 2A5 | Thermo Fisher Scientific | Cat# 14-9965-82; RRID: AB_1548835 |
| Mouse monoclonal anti-GFAP, clone GA5 | Millipore | Cat# MAB360; RRID: AB_11212597 |
| Chicken polyclonal anti-GFP | Aves Labs | Cat# GFP-1020; RRID: AB_10000240 |
| Rabbit polyclonal anti-GPR17 | Cayman | Cat# 10136; RRID: AB_10613826 |
| Mouse monoclonal anti-HA-tag, clone HA-7 | Sigma | Cat# H9658; RRID: AB_260092 |
| Rabbit polyclonal anti-Iba1 | Wako | Cat# 019-19741; RRID: AB_839504 |
| Goat polyclonal anti-Iba1 | Abcam | Cat# ab5076; RRID: AB_2224402 |
| Rabbit anti-Laminin-1 | Sigma | Cat# L9393; RRID: AB_477163 |
| Mouse monoclonal anti-Myc-tag, clone 9E10 | Sigma | Cat# 05-419; RRID: AB_309725 |
| Mouse monoclonal anti-Nestin, clone rat-401 | Millipore | Cat# MAB353; RRID: AB_94911 |
| Mouse monoclonal anti-NeuN | Millipore | Cat# MAB377; RRID: AB_2298772 |
| Rabbit polyclonal anti-NG2 | Millipore | Cat# AB5320; RRID: AB_11213678 |
| Goat polyclonal anti-PDGFRA | R&D Systems | Cat# AF1062; RRID: AB_2236897 |
| Rat monoclonal anti-PDGFRA, clone APA5 | BD Biosciences | Cat# 558774; RRID: AB_397117 |
| Goat polyclonal anti-PDGFRB | R&D Systems | Cat# AF1042; RRID: AB_2162633 |
| Rat monoclonal anti-PECAM1/CD31 biotin, clone MEC 13.3 | BD Biosciences | Cat# 553371; RRID: AB_394817 |
| Mouse monoclonal anti-alpha-SMA, clone 1A4 | Abcam | Cat# ab7817; RRID: AB_262054 |
| Goat polyclonal anti-SOX10 | R&D Systems | Cat# AF2864; RRID: AB_442208 |
| Rabbit polyclonal anti-TagRFP | Kerafast | Cat# EMU113 |
| **Chemicals, peptides, and recombinant proteins** | | |
| Tamoxifen | Sigma | Cat# T5648 |
| Corn oil | Sigma | Cat# C8267 |
| EdU (5-Ethynyl-2′-deoxyuridine) | Click Chemistry Tools | Cat# 1140 |
| Cytosine β-D-arabinofuranoside | Sigma | Cat# C1768 |
| Artificial cerebrospinal fluid (aCSF) | Tocris Bioscience | Cat# 3525 |
| Phusion® High-Fidelity DNA Polymerase | New England Biolabs | Cat# M0530S |
| Gibson Assembly® Master Mix | New England Biolabs | Cat# E2611S |
| Lipofectamine™ 2000 Transfection Reagent | Thermo Fisher | Cat# 11668019 |
| Streptavidin-Brilliant Violet 480 | BD Biosciences | Cat# 564876 |
| Hoechst 33342, Trihydrochloride, Trihydrate - 10 mg/mL Solution in Water | Thermo Fisher | Cat# H3570 |
| BlokHen® Blocking Reagent | Aves Labs | Cat# BH-1001 |
| **Critical commercial assays** | | |
| Black-Gold II Myelin Ready-to-Dilute Staining Kit | Biosensis | Cat# TR-100-B |
| Click-iT™ Plus EdU Cell Proliferation Kit for Imaging, Alexa Fluor™ 647 dye | Thermo Fisher | Cat# C10640 |

(*Continued on next page*)

CellPress
OPEN ACCESS

*Continued*

| REAGENT or RESOURCE | SOURCE | IDENTIFIER |
|---|---|---|
| Experimental models: Cell lines | | |
| HEK293T cells | Sigma | Cat# 85120602-1VL |
| Experimental models: Organisms/strains | | |
| Mouse: Gt(ROSA)26Sor$^{tm14(CAG-tdTomato)Hze}$ | The Jackson Laboratory | MGI:3809524 |
| Mouse: Gt(ROSA)26Sor$^{tm4(ACTB-tdTomato,-EGFP)Luo}$ | The Jackson Laboratory | MGI:3716464 |
| Mouse: Tg(Nes-cre/ERT2)5-1Kag | Imayoshi et al.[40] | MGI:3641212 |
| Mouse: Tg(Pdgfra-cre/ERT2)1Wdr | Rivers et al.[12] | MGI:3832569 |
| Mouse: Tg(Sox10-GFP,-DTA)1Wdr | Kessaris et al.[20] | MGI:4999728 |
| Recombinant DNA | | |
| CX-nestinGFPas | Addgene | Cat# 32401 |
| pCAG-NLS-HA-Dre | Addgene | Cat# 51272 |
| pEF.myc.ER-E2-Crimson | Addgene | Cat# 38770 |
| FUGW | Addgene | Cat# 14883 |
| FUW-Nestin-NLS-HA-Dre | This paper | N/A |
| FUW-EF1$\alpha$-FREX-Myc/mKate2-f-mem | This paper | N/A |
| pmKate2-f-mem | Evrogen | Cat# FP186 |
| Software and algorithms | | |
| Fiji for macOS (ImageJ2 version 2.3.0/1.53f) | http://fiji.sc | RRID: SCR_002285 |
| GraphPad Prism 9 for macOS (version 9.3.1) | http://www.graphpad.com/ | RRID: SCR_002798 |
| Geneious Prime 2020 | http://www.geneious.com/ | RRID: SCR_010519 |
| SnapGene (version 5.2) | http://www.snapgene.com/ | RRID: SCR_015052 |
| Other | | |
| Alzet osmotic minipump | Alzet | Cat# 1007D |
| NanoFil syringe (10 $\mu$L) | World Precision Instruments | Cat# NANOFIL |
| UMP3 UltraMicroPump | World Precision Instruments | Cat# UMP3-3 |

## RESOURCE AVAILABILITY

### Lead contact

Further information and requests for resources and reagents should be directed to and will be fulfilled by the lead contact, Tobias D. Merson (toby.merson@nih.gov).

### Materials availability

Plasmids generated in this study, namely *FUW-Nestin-NLS-HA-Dre* and *FUW-EF1$\alpha$-FREX-Myc/mKate2-f-mem*, will be made available upon request.

### Data and code availability

- The published article includes all datasets generated during the study.
- This paper does not report original code.
- Any additional information required to reanalyze the data reported in this paper is available from the lead contact upon request.

## EXPERIMENTAL MODEL AND SUBJECT DETAILS

### Animals

Animal experiments were conducted in accordance with the National Health and Medical Research Council guidelines for the care and use of animals. All animal studies were approved by the animal ethics committee of the Florey Institute of Neuroscience and Mental Health (Parkville, VIC, Australia) and the animal ethics committee of Monash University (Clayton, VIC, Australia). Both male and female mice were used in all experimental cohorts, with experimental interventions (i.e. tamoxifen gavage) starting between 8–10 weeks of age. *Pdgfr$\alpha$-CreER$^{T2}$* PAC transgenic mice (MGI:3832569) expressing CreER$^{T2}$ under the regulation of the *Pdgfra* gene promoter, and *Sox10-DTA* transgenic mice (MGI:4999728) expressing a P1-derived artificial chromosome DNA construct containing the gene cassette *Sox10-lox-GFP-poly(A)-lox-DTA* driven by the *Sox10* promoter.[12,20] These two mouse lines were crossed to generate

*Pdgfrα-CreER*$^{T2+/+}$*:Sox10-DTA*$^{+/-}$ and *Pdgfrα-CreER*$^{T2+/+}$*:Sox10-DTA*$^{-/-}$ breeders that were used to produce experimental cohorts comprising male and female offspring. To generate *Pdgfrα-CreER*$^{T2+/-}$*:Sox10-DTA*$^{+/-}$*:Ai14 tdTomato*$^{+/-}$ mice, we crossed *Pdgfrα-CreER*$^{T2+/+}$*:Sox10-DTA*$^{+/-}$ mice with homozygous *Ai14 tdTomato*$^{+/+}$ mice (MGI:3809524), which were purchased from the Jackson Laboratory. We also generated *Nestin-CreER*$^{T2+/-}$*:Pdgfrα-CreER*$^{T2+/-}$*:Sox10-DTA*$^{+/-}$ transgenic mice for the combined ablation of both parenchymal OPCs and oligodendrogenic NPCs by crossing *Pdgfrα-CreER*$^{T2+/+}$*:Sox10-DTA*$^{+/-}$ mice with *Nestin-CreER*$^{T2+/+}$ *(line 5.1)* mice (MGI:3641212)[40] generously provided by Ryoichiro Kageyama. We noted that a number of *Nestin*$^{+}$*:Pdgfra*$^{+}$*:DTA*$^{+}$ mice did not survive beyond weaning due to hydrocephalus. In surviving adult mice that were administered TAM and AraC (n=3 mice), we observed anatomical abnormalities consistent with hydrocephalus including expanded lateral ventricles (Figures S5J and S5K). Hydrocephalus was noted in *Nestin*$^{+}$*:Pdgfra*$^{+}$*:DTA*$^{+}$ mice as early as postnatal day 16. The ratio of *Nestin*$^{+}$*:Pdgfra*$^{+}$*:DTA*$^{+}$ versus *Nestin*$^{+}$*:Pdgfra*$^{+}$*:DTA*$^{-}$ mice surviving beyond weaning (P21) was 33.6% (36 out of 107 offspring) and gross hydrocephalus was evident in 39% of mice (14/36 mice) that survived post weaning. By contrast, no *Nestin*$^{+}$*:Pdgfra*$^{+}$*: DTA*$^{-}$ mice exhibited evidence of gross hydrocephalus (0/71 mice). The incidence of hydrocephalus in *Nestin*$^{+}$*:Pdgfra*$^{+}$*:DTA*$^{+}$ mice likely reflects TAM-independent recombination of the DTA allele due to leaky Cre activity driven by the *Nestin-CreER*$^{T2}$ allele during ontogeny thereby resulting in congenital apoptosis of a subset of neural crest cells[40] which express both SOX10 and Nestin.[41] This possibility is supported by the observation that loss of neural crest cells during fetal development is documented to cause hydrocephalus.[42,43] Finally, we generated *Nestin-CreER*$^{T2+}$*: mTmG*$^{+}$ mice to evaluate the degree of TAM-independent recombination among adult neural progenitor cells by crossing *Nestin-CreER*$^{T2+/+}$ *(line 5.1)* mice with *mTmG*$^{+/+}$ mice (MGI:3716464).

## METHOD DETAILS

### Timelines of experimental interventions for high-efficiency OPC ablation

*Step 1*: Starting at 8–10 weeks of age, *Pdgfrα*$^{+}$*:DTA*$^{+}$ mice receive TAM by oral gavage for 4 consecutive days. *Step 2:* Starting 4 days after the last day of TAM gavage, mice undergo surgical implantation of an osmotic minipump to deliver AraC into the CSF via the cisterna magna. *Step 3:* After 6 days of intracisternal infusion, mice undergo surgery to remove the osmotic minipump. The day of minipump removal is recorded as 0 days post-pump removal (0 dppr). *Step 4:* Mice are humanely sacrificed by perfusion fixation at the desired time-point, noting that OPCs remain depleted in the brain until at least 10 dppr.

### TAM gavage

Cre-mediated recombination was induced by oral gavage of TAM (Sigma) delivered at a dose of 300 mg/kg/d for 4 consecutive days, as described in previous studies.[12,33] TAM was prepared at 40 mg/mL in corn oil (Sigma). No toxicity due to TAM administration was observed in any cohort of mice.

### EdU administration

To label cells that proliferated during the first 10 days following AraC withdrawal, 5-ethynyl-2′-deoxyuridine (EdU; Life Technologies) was administered to mice in their drinking water at 0.1 mg/mL. EdU-supplemented drinking water was placed in light-proof water bottles and replaced every 3 days.

### Preparation of AraC for intracisternal infusions

Cytosine-β-D-arabinofuranoside (AraC, Sigma) was prepared at a final concentration of 2% (w/v) in artificial CSF (aCSF, Tocris Bioscience). One hundred microliters of either 2% AraC or vehicle (aCSF) was injected into osmotic minipumps (Alzet Model 1007D, flow rate 0.5 μL/h, Brain Infusion Kit III) using a 1 mL syringe attached to a blunt fill needle. The flow moderator was attached to a bespoke tubing assembly made by connecting PE-10 polyethylene tubing to the vinyl catheter tube provided with the Brain Infusion Kit III (Alzet). The flow moderator with attached tubing was slowly inserted into the filled osmotic minipump to create a complete pump assembly. The pumps were then transferred into 50 mL conical tubes containing sterile saline and placed in a 37°C water bath overnight to prime the pumps prior to surgical implantation.

### Surgical implantation of osmotic minipumps

AraC or vehicle (aCSF) was infused into the CSF at the level of the cisterna magna via an osmotic minipump for a period of 6 days. Prior to anesthesia, mice received a subcutaneous injection of meloxicam (2 mg/kg, 0.25 mL/10 g body weight) in warm saline. Mice were then anesthetized by isoflurane inhalation (4% induction, 2% maintenance). The head of the anesthetized mouse was fixed in a stereotaxic frame using a nose cone and ear bars. The position of the abdomen was lowered so that the neck was flexed at an angle of 30–45° relative to horizontal and the body was placed on a thermostatically controlled heat pad to maintain body temperature. Eyes were moistened with water-based lubricant and the fur was cleared over the head and shoulders with an electric shaver. A sterile cotton tip soaked in 80% ethanol was used to swab and clean the surface of incision site, followed by 10% (w/v) povidone-iodine solution (Betadine). A midline skin incision was made using a sharp scalpel from a position just rostral of the external occipital protuberance to ~1 cm cranial to the shoulders. The atlanto-occipital membrane was visualized after blunt dissection of the muscle layers to expose the position of the cisterna magna. Using a straight hemostat, a pocket was created by spreading the subcutaneous connective tissues apart and the osmotic minipump was inserted into the pocket overlying the hindquarters. The cisterna magna was

pierced superficially with a 25 G needle and the PE-10 tubing connected to the osmotic minipump was introduced into the hole before applying a small amount of superglue to fix the tubing in place. The position of the tubing was further anchored and fixed to the musculature using sutures. Bupivacaine (100 μL of 0.25% solution) was flushed over the musculature to provide rapid onset analgesia. The skin was then sutured and 10% (w/v) povidone-iodine solution was applied to the sutured skin. The animal was placed in a warm recovery box for monitoring until it regained consciousness and normal mobility. Animals were monitored daily throughout the experiment and were administered meloxicam (2 mg/kg, 0.25 mL/10 g body weight) in warm saline once daily for the first 2 days post-surgery. All mice were provided with powdered chow mixed with fresh water daily in a small dish that was easily accessed within the animal cage.

### Surgical removal of osmotic minipumps

Infusion of AraC or vehicle (aCSF) was ceased after 6 days by removing the osmotic minipumps. Animals were anesthetized as described above and the former skin incision site was reopened to gain access to the tubing connected to the osmotic minipump. The tubing was cut 2 mm from the glued/sutured musculature and the minipump was removed from the subcutaneous pocket. The tubing fixed to the musculature was left in place and the free end of the tubing was sealed with superglue. The incision was closed with sutures and the animal was placed in a warm recovery box for monitoring until it regained consciousness and normal mobility. Animals were monitored daily throughout the experiment. AraC-administered mice experienced a mild reduction in body weight during AraC infusion. If mice showed signs of greater than 10% weight loss, they were given powdered chow mixed with fresh water daily in a small dish that was easily accessed within the animal cage. If mice maintained greater than 15% weight loss for more than 72 h, they were humanely euthanized. Following removal of the osmotic minipumps delivering AraC, mice returned to normal weight.

### Generation of lentiviral vectors

The lentiviral vectors *LV-FUW-Nestin-NLS-HA-Dre* and *LV-FUW-EF1α-FREX-Myc/mKate2-f-mem* were used for fate-mapping of V-SVZ-derived NPCs. These vectors were designed using Geneious Prime bioinformatics software (RRID: SCR_010519) and constructed using standard molecular cloning techniques, including PCR using Phusion High-Fidelity DNA polymerase (New England Biolabs), restriction enzyme digestion and Gibson assembly (New England Biolabs). To create these lentiviral vectors, the rat *Nestin* promoter sequence was amplified by PCR from plasmid DNA (Addgene Cat#32401). The DNA encoding *NLS-HA-Dre* was amplified by PCR from plasmid DNA (Addgene Cat#51272). The coding sequence for the rat *Nestin* second intron enhancer was amplified from rat genomic DNA. *EF1α* promoter sequence was amplified by PCR from plasmid DNA (Addgene Cat#38770). The *FREX-Myc/mKate2-f-mem DNA* sequence was generated by DNA synthesis (Integrated DNA Technologies). The PCR products were cloned into the FUGW lentiviral vector backbone (Addgene Cat#14883) in place of the GFP coding sequence by Gibson Assembly. Plasmid DNA was then extracted and purified using Plasmid Mini or Midi Kits (Qiagen). The DNA sequences of the lentiviral vectors were verified by Sanger sequencing (Micromon, Monash University). Sequence alignments were performed using SnapGene molecular biology software (RRID: SCR_015052).

### *In vitro* validation of lentiviral vectors

Plasmid DNA was transfected into HEK293T cells cultured at 37°C and 5% $CO_2$ and analyzed 48 h post-transfection for fluorescence. The *pmKate2-f-mem* plasmid (Evrogen Cat#FP186) served as a positive control for mKate2 fluorescence. HEK293T cells were plated in a 24-well plate and cultured in Dulbecco's Modified Eagle's Medium (DMEM, Gibco), supplemented with 10% fetal bovine serum (Invitrogen). At 80% confluency, cells were transfected with the plasmids using Lipofectamine 2000 Transfection Reagent (Thermo Fisher) according to the manufacturer's instructions. The growth medium was replaced with fresh medium containing 100 U/mL penicillin and 100 mg/mL streptomycin (Gibco) 4 h post-transfection. At 48 h after transfection, cells were post-fixed with 4% PFA/DPBS, processed for immunocytochemistry and imaged for mKate2 expression using a Zeiss LSM780 confocal microscope.

### Lentivirus production

Lentiviruses were produced and packaged in HEK293T cells by the Vector and Genome Engineering Facility, Children's Medical Research Institute (Westmead, Australia). To determine viral titer, HEK293T cells were transduced with lentivirus. Genomic DNA was extracted from transduced cells and viral DNA copy number/cell was determined by Multiplex Taqman qPCR.

### Intraventricular injection of lentiviral vectors

Mice were anesthetized by isoflurane inhalation and positioned in a motorized stereotaxic frame as described above. A small incision was made in the scalp and the injection site of the lateral ventricle was marked using the following stereotaxic coordinates, relative to bregma: anterior-posterior −0.22 mm, medial-lateral −1.00 mm, and dorsal-ventral −2.5 mm. A small hole was drilled into the skull to expose the brain surface. Five microliters of mixed lentiviral vectors were gently drawn up into a blunt-tipped 35G needle attached to a 10 μL NanoFil syringe (World Precision Instruments, WPI). The syringe was then placed into a microinjection pump (UltraMicroPump III, WPI) attached to the stereotaxic frame and lowered slowly into the injection site of the lateral ventricle according to the dorsal-ventral coordinate. The microinjection pump controlled the infusion of 5 μL total volume of lentiviruses at a flow rate of 0.5 μL/min, after which the needle was left in place for 5 min to ensure complete diffusion of the viruses and avoid backflow.

### Tissue processing and immunohistochemistry

Mice were deeply anesthetized with 100 mg/kg sodium pentobarbitone and then transcardially perfused with PBS, followed by 4% PFA/PBS. Brains, optic nerves and spinal cords were removed and post-fixed in 4% PFA/PBS for 2 h on ice, transferred to PBS overnight, cryopreserved in 20% sucrose/PBS overnight, followed by embedding in Tissue-Tek OCT compound (Sakura FineTek). The tissues were stored at −80°C until sectioned. Ten micron-thick coronal sections of the brain and spinal cord, and longitudinal sections of the optic nerve were cut on a Leica cryostat, collected onto Superfrost Plus slides (Menzel Glaser), and air dried for 1 h before storing at −80°C until stained. Cryosections were air dried, then blocked with PBS containing 0.3% Triton X-100, 10% normal donkey serum, and 10% BlokHen (Aves Labs Cat. BH-1001) for 1 h at room temperature (RT). The sections were then incubated with primary antibodies at RT overnight, followed by 1 h incubation at RT with secondary antibodies.

For multiplex immunohistochemistry, some primary antibodies were incubated simultaneously. The following primary antibodies were used: rabbit anti-ALDH1L1 (1:1000, Abcam Cat# ab87117), rabbit anti-ASPA (1:500, GeneTex GTX113389), mouse anti-CC1 (1:100, Calbiochem Cat# OP80), rat anti-CD16/CD32 (1:100, BD Biosciences Cat# 553142), rabbit anti-CD206 (1:200, Abcam Cat# ab64693), goat anti-DCX (1:100; Santa Cruz Biotechnology Cat# sc-8066), mouse anti-FoxJ1 (1:200, eBioscience Cat# 14-9965-82), mouse anti-GFAP (1:500, Millipore Cat# MAB360), chicken anti-GFP (1:2000, Aves Labs Cat# GFP-1020), rabbit anti-GPR17 (1:800, Cayman Cat# 10136), mouse anti-HA-tag (1:500, Sigma Cat# H9658), rabbit anti-Iba1 (1:200, Wako Cat# 019-19741), goat anti-Iba1 (1:500, Abcam Cat# ab5076), rabbit anti-Laminin-1 (1:400, Sigma Cat# L9393), mouse anti-Myc-tag (1:500, Sigma Cat# 05-419), mouse anti-Nestin (1:100, Millipore Cat# MAB353), mouse anti-NeuN (1:100, Millipore Cat# MAB377), rabbit anti-NG2 (1:200, Millipore Cat# AB5320), goat anti-PDGFRA (1:150, R&D Systems Cat# AF1062), rat anti-PDGFRA (1:150, BD Biosciences Cat# 558774), goat anti-PDGFRB (1:200, R&D Systems Cat# AF1042), mouse anti-α-SMA (1:500, Abcam Cat# ab7817), goat anti-SOX10 (1:100, R&D Systems Cat# AF2864), and rabbit anti-TagRFP for mKate2 labeling (1:500, Kerafast Cat# EMU113). To label $GFP^+$ $tdTomato^+$ brain sections using primary antibodies against Nestin, PDGFRA, and NG2, as well as EdU and Hoechst, inactivation of GFP and tdTomato was performed by firstly treating the brain sections with 3% $H_2O_2$ and 20 mM HCl in PBS for 1 h at RT with light illumination.[44] The slides were then washed three times with PBS, incubated with blocking buffer and processed for the immunostaining as described above.

Secondary antibodies raised in donkey and conjugated to Alexa Fluor 488, FITC, TRITC, Alexa Fluor 594 or Alexa Fluor 647 were purchased from Jackson ImmunoResearch or Invitrogen and used at 1:200 dilution. Sections incubated with biotinylated rat anti-PECAM1/CD31 antibody (1:200, BD Biosciences Cat# 553371) were rinsed and further incubated with streptavidin-Brilliant Violet 480 (1:200; BD Biosciences Cat# 564876) for 30 min. Some slides stained without the fluorophore Brilliant Violet 480 were also counterstained with Hoechst 33342 (1 μg/mL, Thermo Fisher).

For myelin analysis, slides were stained with Black-Gold II (Biosensis) according to the manufacturer's instructions. To detect EdU incorporation in proliferating cells, sections were first processed for immunohistochemistry as above, followed by EdU detection using the Click-iT EdU Alexa Fluor 647 Imaging Kit (Thermo Fisher) as per the manufacturer's instructions. Sections were coverslipped with Mowiol mounting medium and subjected to fluorescence and confocal microscopic analysis.

### Imaging

Stained 10 μm thick coronal sections were imaged by laser scanning confocal microscopy (Zeiss LSM510-META or Zeiss LSM780), which was used to detect up to four fluorophores by laser excitation at 405, 488, 561 and 633 nm wavelengths. For five-color imaging such as brain sections stained with Brilliant Violet 480 or Hoechst, as well as Alexa Fluor 488, TRITC, Alexa Fluor 594 and Alexa Fluor 647, linear unmixing was performed during acquisition (online fingerprinting). Tile scanning was performed at a magnification of 10x or 20x for the cellular analysis of the entire brain sections of transgenic mouse lines. For the analysis of Laminin-1/PDGFRA, NG2/PDGFRA or PDGFRB/PDGFRA colocalization, confocal images were acquired using a 63X objective to generate Z-stacks.

For global analysis of cellular distributions in the entire mouse brain, 2–3 sections at each rostro-caudal position were scanned on an Olympus VS120 Virtual Slide Microscope with a 20x objective at Monash Histology Platform, Monash University. The resulting images have a pixel resolution of 0.65 μm/pixel.

For the sections stained with Black-Gold II, 2–3 representative images per mouse were taken using a 10x objective on a Zeiss Axioplan upright fluorescent microscope and captured with an Axioplan HRc camera (Carl Zeiss) using the Axiovision 7.2 imaging software. All images were taken with the same exposure time.

### Image processing

Confocal images were imported into Fiji image analysis software (Fiji for macOS, RRID: SCR_002285) for quantification of cellular density in the regions of interest. For image stacks, deconvolution was performed with the "Iterative Deconvolve 3D" plugin in Fiji. Colocalization analysis was performed by using the "Colocalization threshold" plugin in Fiji to automatically determine a detection threshold for each channel to avoid subjective bias. The extent of within-pixel fluorescent signal colocalization as indicated by Pearson's correlation coefficient was calculated in each optical slice and then flattened into a maximal Z-projection to reveal colocalized pixels across the entire image thickness. All analyses were performed in a blinded fashion.

CellPress
OPEN ACCESS

## QUANTIFICATION AND STATISTICAL ANALYSIS

### Image analysis and cell quantification

For slide-scanned images, double- or triple-positive cells were counted manually in Fiji. For morphological analysis of microglia and astrocytes, Z-stacks of 1–4 cells were taken from the cortical region of each of the brain sections under a 40× objective. Microglia soma and branching measures were visualized using IBA1 immunofluorescence, whereas those for astrocytes were assessed with GFAP. Z-stacked images were converted to maximum intensity projections using Fiji and these images were background subtracted, contrast-enhanced to ensure full arborization could be detected and a local threshold was applied to the image. Microglial and astrocytic soma areas were calculated using the 'Measure' command and branch features (number of primary or secondary processes; maximum length of primary process) were manually counted and measured in Fiji. A total of 18–22 astrocytes and 18–39 microglia per group were analyzed in a blinded fashion. For quantification of myelin intensity, images from the sections stained with Black-Gold II were converted to grayscale in Fiji and automated measurements of myelin intensity were taken using the measurement function to record the mean gray value within the regions of interest. All analyses were performed in a blinded fashion.

### Probability calculations

At 0 dppr, we did not find any PDGFRA$^+$ OPCs in sections of the cerebrum of TAM + AraC-administered *Pdgfrα*$^+$*:DTA*$^+$ mice that were examined. However, since we did not analyze every single section of each mouse brain, we cannot exclude the possibility that there could be undetected OPCs in sections of the brains of OPC-ablated mice that were not examined. To estimate the theoretical number of undetected OPCs that could be missed based on our tissue sampling strategy, we calculated the probability that the cerebrum of sampled tissue sections contains no OPCs in circumstances where residual OPCs are sparsely distributed across the cerebrum. For OPC-ablated mice, we performed cell counts using six (6) ten-micron thick sections per mouse for a total of 4 mice at 0 dppr, i.e., a total of 24 sections across the 4 mice. These sections were sampled from a region of interest (ROI) extending from +0.25 mm to −5.07 mm A/P relative to bregma, theoretically reflecting a total of 532 ten-micron thick sections per mouse. We calculated the probability of detecting zero OPCs in the cerebrum of randomly sampled sections under various conditions, where we defined the number of sections ($N$) that contain no OPCs in the region of the cerebrum from which the sections were collected. The probability ($P_1$) of selecting 6 sections that contain no OPCs is given by the formula $\left[P_1 = \left(\frac{N}{532}\right) \times \left(\frac{N-1}{531}\right) \times \left(\frac{N-2}{530}\right) \times \left(\frac{N-3}{529}\right) \times \left(\frac{N-4}{528}\right) \times \left(\frac{N-5}{527}\right)\right]$. Since we selected 6 sections from each of 4 mice, then the probability ($P_2$) of selecting a total of 24 sections that contain no OPCs is given by the formula $[P_2 = (P_1)^4]$. The percentage ($X$) of sections devoid of OPCs was calculated as $\left[X = \left(\frac{N}{532}\right) \times 100\right]$. We plotted $P_2$ against $X$ (Figure S1E) and determined the value of $N$ when $\underline{P_2} = 0.5$. Finally, we calculated the number of sections ($S$) that contain OPCs when $P_2 = 0.5$ using the formula $[S = 532 - N]$, which gave a value of 15 sections per ROI. Working on the assumption that the cerebrum in each of these sections contains one OPC, we estimated that there are likely to be fewer than about 15 OPCs within the cerebrum ROI for each OPC-ablated mouse.

### Statistical analyses

All statistical analyses were performed using the GraphPad Prism software (v.9). Statistical significance was determined using an unpaired, two-tailed Student's t test or by two-way ANOVA with Bonferroni's, Tukey's or Sidak's multiple-comparison tests. Statistical significance was defined as $p < 0.05$. Quantitative data are reported as mean ± SEM.